RSC Advances

REVIEW

View Article Online
View Journal | View Issue

Cite this: *RSC Adv.*, 2022, **12**, 20360

Synchrotron radiation based X-ray techniques for analysis of cathodes in Li rechargeable batteries†

Jitendra Pal Singh, [ab] Anil Kumar Paidi, [a] Keun Hwa Chae, [c] Sangsul Lee *[ad] and Docheon Ahn *[a]

Li-ion rechargeable batteries are promising systems for large-scale energy storage solutions. Understanding the electrochemical process in the cathodes of these batteries using suitable techniques is one of the crucial steps for developing them as next-generation energy storage devices. Due to the broad energy range, synchrotron X-ray techniques provide a better option for characterizing the cathodes compared to the conventional laboratory-scale characterization instruments. This work gives an overview of various synchrotron radiation techniques for analyzing cathodes of Li-rechargeable batteries by depicting instrumental details of X-ray diffraction, X-ray absorption spectroscopy, X-ray imaging, and X-ray near-edge fine structure-imaging. Analysis and simulation procedures to get appropriate information of structural order, local electronic/atomic structure, chemical phase mapping and pores in cathodes are discussed by taking examples of various cathode materials. Applications of

Received 24th February 2022
Accepted 15th June 2022

DOI: 10.1039/d2ra01250b

rsc.li/rsc-advances

[a]*Pohang Accelerator Laboratory, Pohang University of Science and Technology, Pohang-37673, Republic of Korea. E-mail: sangsul@postech.ac.kr*

[b]*Department of Physics, Manav Rachna University, Faridabad-121004, Haryana, India*

[c]*Advanced Analysis Center, Korea Institute of Science and Technology, Seoul-02792, Republic of Korea*

[d]*Xavisoptics, Pohang-37673, Republic of Korea*

† Electronic supplementary information (ESI) available. See https://doi.org/10.1039/d2ra01250b

Jitendra Pal Singh is currently working at Manav Rachna University as a Ramanujan Fellow. He received Ph.D. from Govind Ballabh Pant University of Agriculture and Technology, Pantnagar, Uttarakhand in 2010. He worked as a Research Associate at Inter-University Accelerator Centre, New Delhi, during 2010–2011 and as a post-doc researcher at Taiwan SPIN Research Centre, National Chung Cheng University, Taiwan, during 2011–2012. He was an Assistant Professor at Krishna Engineering College, Ghaziabad, India, from 2012 to 2014. In 2014, he joined the Korea Institute of Science and Technology, Korea. He moved to Pohang Accelerator Laboratory, Pohang, South Korea and worked there from December 2018 to May 2022. His research interests are irradiation studies in nanoferrites, thin films, magnetic multilayers, biomaterials and cathode materials. He has expertise in X-ray absorption spectroscopy and hard X-ray imaging. Dr Singh is a member of Magnetic Society of India, Indian Physics Association, and Ion Beam Society of India.

Anil K. Paidi earned his Ph.D. in Solid State Chemistry, Inorganic Chemistry Division under Prof. K. Vidyasagar from the Indian Institute of Technology Madras, India. Subsequently, he performed postdoctoral work under Prof. A. Mukhopadhyay's group (Indian Institute of Technology Bombay, India). Dr Paidi is currently a postdoctoral researcher, working with Dr Dochean Ahn and Dr Sangsul Lee at Pohang Accelerator Laboratory, South Korea. His research primarily focuses on understanding the chemistry that is relevant to energy storage materials. He is currently working on nickel-rich layered transition metal oxide compositions for high-capacity cathodes.

these synchrotron techniques are also explored to investigate oxidation state, metal–oxygen hybridization, quantitative local atomic structure, Ni oxidation phase and pore distribution in Ni-rich layered oxide cathodes.

Introduction

In recent years, the development of electrochemical devices with improved performance has received significant attention for fulfilling the increased energy demand of mankind.[1,2] This necessity leaves researchers to optimize these devices in terms of cost-effectiveness and energy consumption.[3–5] A battery is a fine example of an electrochemical energy device that stores chemical energy and converts it into electrical energy. The energy conversion takes place due to the occurrence of redox reactions at the anode and cathode.[6] Thus, a typical battery consists of an anode and a cathode separated by an electrolyte (Fig. 1a and b).[6,7]

Fig. 1a shows a schematic of the primary battery which contains an immersed anode in the electrolyte surrounded by the cathode. In this case, electrical energy is produced by the movement of ions in the electrolyte. This kind of battery is also known as a primary battery as it is usually discarded after use.[8,9] Thus, commercial use of this battery is limited to household appliances.[10]

Another battery that is based on the same phenomenon but can be charged again after being discharged is known as a rechargeable or secondary battery (Fig. 1b).[11–13] The term "accumulator" is also used for this battery as it accumulates and stores energy through a reversible electrochemical reaction. This battery can be re-used after discharging which makes it suitable for long term use. Thus, it is utilized for numerous appliances – ranging from portable devices[14,15] to electrical vehicles (EV)[16–19] (Fig. 1c), thereby helping to fulfill the increased energy demands of mankind.

Rechargeable batteries are designed and named based on several combinations of electrodes and electrolytes. Some of these batteries are lead–acid,[20] nickel–cadmium (NiCd),[21] nickel–metal hydride (NiMH),[22] lithium-ion (Li-ion),[23] and lithium-ion polymer (Li-ion polymer).[24] Li-ion rechargeable batteries (LIB)[25,26] received significant attention from the scientific community in recent years owing to superior electrochemical performance.[27–29]

Li-ion rechargeable batteries (LIB)

LIB is a type of rechargeable battery in which lithium ions (Li^+) move from the cathode to anode during charging and *vice versa* when discharging. As can be seen from the Ragone plot of energy devices, the performance of LIBs is just below the traditional combustion engine (Fig. 2a).[30,31] This plot also informs that LIBs have better energy density and power density compared to not only to other rechargeable batteries but also to another sources of electricity storage such as capacitors. This

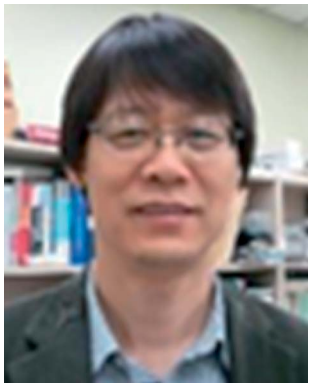

Keun Hwa Chae received a B.Sc. in physics in 1986 and an M.Sc. in Physics in 1988 from Yonsei University, Seoul, Korea. In 1994, he received Ph.D. Degree in Physics from Yonsei University, Seoul, Korea. He was a post-doctoral fellow from 1995-97 at Rutgers-The State University of New Jersey, USA. His research fields are ion beam modification of materials and characterization of materials using synchrotron radiation. He has been working as a principal research scientist in Korea Institute of Science and Technology, Korea, since 2000.

Sangsul Lee is the head of the PAL-EUV metrology and inspection at Pohang Accelerator Laboratory, POSTECH. He is also the chief technology officer of Xavisoptics, an X-ray solution, and equipment company. He received Ph.D. in materials science and engineering from Hanyang University in 2012. His research interest is synchrotron-based nanoscale imaging such as EUV metrology, inspection, and nanoscale tomography.

Docheon Ahn is a senior scientist and manager of 9B high resolution powder diffraction beamline at Pohang Accelerator Laboratory (PAL). He received his Ph.D. in materials science & engineering from Pohang University of Science and Technology (POSTECH) in 2010. He was a visiting scientist at Advanced Photon Source (APS) of Argonne National Laboratory (ANL) in 2017. His primary research focuses on crystal structural analysis using X-ray powder diffraction and development of electrode materials for rechargeable batteries. He is the author of more than 100 peer-reviewed papers.

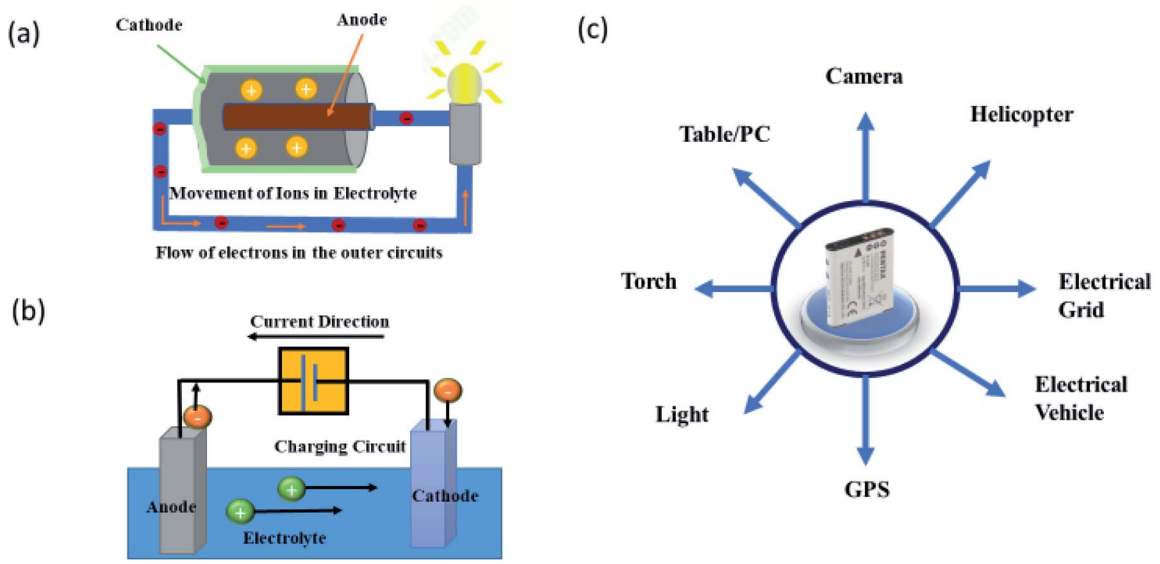

Fig. 1 (a) Primary battery showing the electricity generation through the movement of electrons *via* electrolyte. Adapted from https://www.explainthatstuff.com/batteries.html. (b) Schematic of rechargeable batteries. Adapted from https://www.matsusada.com/column/battery_chaege-dischaege.html. (c) Applications of rechargeable battery. Adapted from https://www.lithiumbatterychina.com/blog/2019/03/21/how-to-find-the-right-custom-lithium-ion-battery-packs-manufacturers-from-china-for-electronic-devices/

makes these batteries prominent candidates to use them as fundamental devices for sustainable energy development.[32–34]

A typical LIB consists of a cathode composed of Li ions as constituents such as $LiNi_{1/3}Co_{1/3}Mn_{1/3}O_2$ (NCM333) and an anode (example, graphite) separated by an electrolyte along with a separator (Fig. 2b).[35,36] Efforts to develop commercially successful LIBs for EVs[37,38] and large-scale grid storages are under process.[39,40] This reflects from the researchers' keen interest in understanding electrochemistry of LIBs by varying cathodes[38,41–44] and anodes[38,44,45] with the impression that electrochemistry plays a key role in the quest for better performance of electrochemical energy storage devices.[46] Some of these

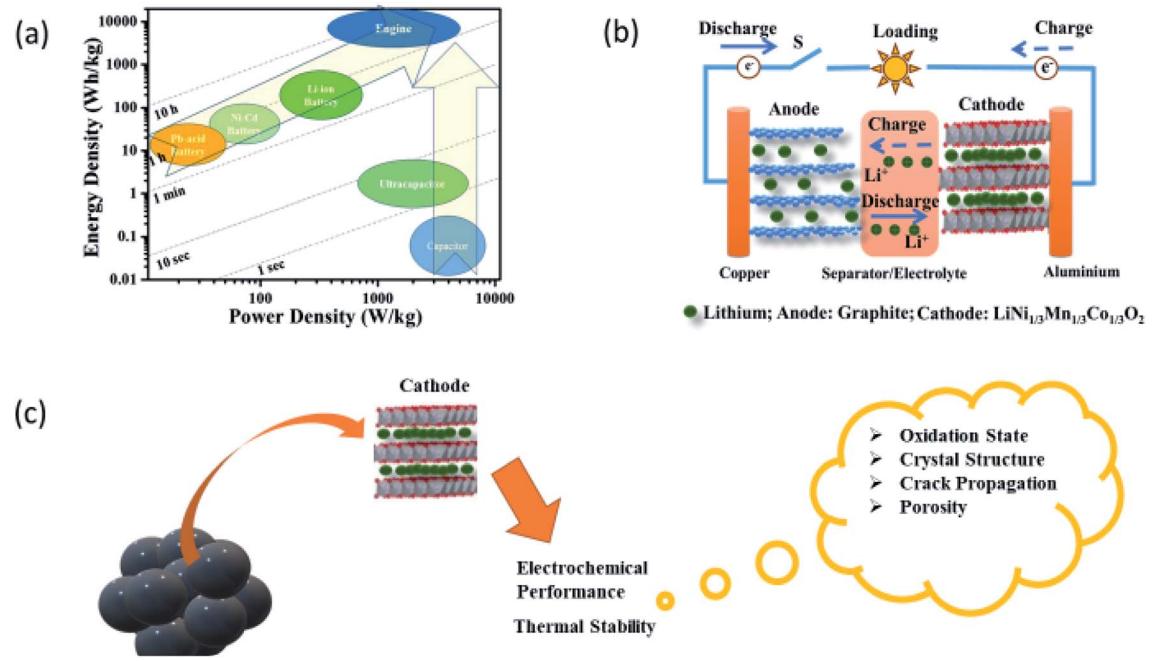

Fig. 2 (a) Ragone plot for energy storage devices and traditional internal-combustion engine. Times shown are the time constants of the devices, obtained by dividing the energy density by the power density. Reproduced from ref. 30 with permission from [Springer Nature], copyright [2021]. (b) Schematic of a typical Li-rechargeable battery and it's various components. Reproduced from ref. 35 with permission from [Elsevier], copyright [2013]. (c) Issues that need attention in cathodes for the improved electrochemical performance of Li-rechargeable battery.

Table 1 Characteristics of representative intercalation cathode compounds; crystal structure, theoretical/experimental/commercial gravimetric and volumetric capacities, average potentials and level of development. Reproduced from ref. 36 with permission from [Elsevier], copyright [2015]

		Theoretical/experimental			
Crystal structure	Materials	Specific capacity (mA h g^{-1})	Volume capacity (mA h cm^{-3})	Average voltage	Ref.
Layered	$LiTiS_2$	225/210	697	1.9	58
	$LiCoO_2$	274/148	1363/550	3.8	59
	$LiNiO_2$	275/150	1280	3.8	60
	$LiMnO_2$	285/140	1148	3.3	61
	$LiNi_{0.33}Mn_{0.33}Co_{0.33}O_2$	280/160	1333/600	3.7	62
	$LiNi_{0.8}Mn_{0.15}Al_{0.05}O_2$	279/199	1284/700	3.7	63
	$Li_2Mn_2O_3$	458/180	1708	3.8	64
Spinel	$LiMn_2O_4$	148/120	596	4.1	65
	$LiCo_2O_4$	142/84	704	4.0	66
Olivine	$LiFePO_4$	170/165	589	3.4	67
	$LiMnPO_4$	171/168	567	3.8	68
	$LiCoPO_4$	167/125	510	4.2	69
Tavorite	$LiFeSO_4$	151/120	487	3.7	70
	$LiVPO_4$	156/129	484	4.2	71

anodes which are investigated so far are Li metal,[47] Si nanoparticles,[48] and $NiFeOPO_4$/C anodes.[49,50]

The electrochemical behavior of Li-rechargeable batteries is extensively studied, focusing on the layered structured cathodes and their compatibility with anodes along with chemical intercalation process to produce high-energy power density.[51–55] One condition for cathode is that they should provide sufficient lattice sites to store and release Li-ions, while maintaining stable cyclability and high specific capacity. Thus, numerous cathodes are developed owing to this concept. Crystal structure, specific capacity, volume capacity and average voltage of a few important cathodes are shown in Table 1.[11,35,36,41] It can be seen clearly seen, that cathodes based on nickel cobalt manganese (NCM) oxide are more suitable[56,57] because of high specific and volume capacity.[11,42–44]

NCM oxides exhibit layered structure, which is suitable for the de-lithiation and lithiation process.[72,73] In the early days, these oxides having Ni, Co, and Mn ratio of 1 : 1 : 1 (*i.e.*, NCM333) were extensively studied.[74–76] Later, it is reported that excess of Ni significantly affects the electrochemical performance.[77–79] Recent reports reveal that Ni-rich cathodes ($LiNi_xMn_yCo_{1-x-y}O_2$; $X \geq 0.9$)[80–83] are better choice among other NCM compositions because of their high cumulative capacity. However, capacity retention is an issue in these cathodes which affects the overall electrochemical performance of LIBs. Besides the electrochemical performance, the thermal stability of cathode material (Fig. 2c) is another important parameter that needs to be taken care of while designing a cathode.[84–86] These aspects in Ni-rich layered oxides are currently receiving significant attention and providing ample scope to the researchers of different communities for carrying out research activities in this direction. Synchrotron community is making a significant impact by solving various issues in cathodes and developing advanced techniques to achieve these objectives. Here, we summarize the recent progress by this community in the context of Ni-rich cathodes by giving an introduction to various synchrotron-assisted techniques.

Synchrotron radiation is an electromagnetic radiation emitted when relativistic charged particles are accelerated radially.[87,88] This radiation is produced artificially in accelerators based on storage ring[89,90] by using bending magnets,[91] undulators and/or wigglers.[92] Main characteristics of this

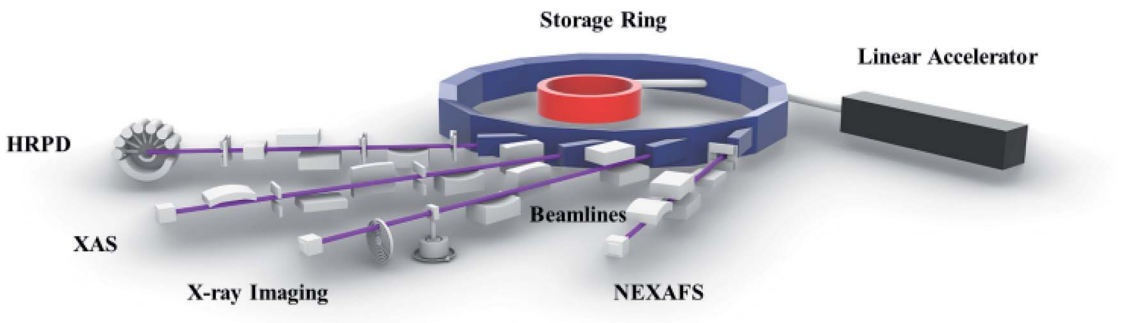

Fig. 3 Various parts of synchrotron radiation source along with schematic of high-resolution powder diffraction (HRPD), X-ray absorption spectroscopy (XAS), X-ray imaging, and near edge X-ray absorption fine structure spectroscopy (NEXAFS) beamlines.

radiation are polarization, and the presence of wavelengths over the entire electromagnetic spectrum.[87–93] It also exhibits high brilliance, a high level of polarization (linear, elliptical, or circular), and high collimation.[94,95] Low emittance, wide tunability in energy/wavelength by monochromatizating (sub-eV up to the MeV range), and pulsed light emission. These characteristics make this radiation more suitable for studying the material behavior compared to other radiations.[96,97] A typical synchrotron radiation source consists of the following parts – (1) linear accelerator, (2) storage ring, and (3) beamline (Fig. 3). This radiation is allowed to travel towards the experimental end station by using beamlines.[98]

Several facilities are established worldwide to produce synchrotron radiation in a wide range of energy, *i.e.*, 100 eV to 50 keV.[99,100] These facilities consist of several characterization techniques such as X-ray photoelectron spectroscopy (XPS) and X-ray absorption spectroscopy (XAS).[101] XPS gives chemical information of elements in the materials.[102,103] XAS is able to probe the local atomic structure along with revealing the oxidation state of core atoms.[104–107] High-resolution photoemission spectroscopy (HRPS) is efficient in examining the band structure.[108] X-ray magnetic circular dichroism (XMCD) provides an opportunity to get insights into the local magnetic structure.[109,110] X-ray reflectivity (XRR) and X-ray scattering (XRS) are used for elucidating dynamics of ordered and disordered materials.[111] Even though depicting almost all aspects of materials, synchrotron techniques could not depict information of spatially resolved characteristics until the early years of this century.[101,104,108,109] Thus, this drawback is overcome by utilizing spatially resolved accessories.[112] XRD-imaging,[113] XANES-imaging,[114] and magnetic-imaging[115] are the results of such efforts. These techniques can provide chemical and structural information of individual clusters of specific sizes decided by spatial resolution of particular facility.[116,117] Thus, this review article gives an overview of XRD, XAS and XANES-imaging technique that are used for assessment of cathodes.[118–123] Apart from this, X-ray imaging is too included in this study.[124,125] A concise discussion of the phenomena investigated using these techniques is also elaborated.

Structural information

Synchrotron-based XRD provides a better way to understand the structural behavior of materials.[126–130] The optical layout of high-

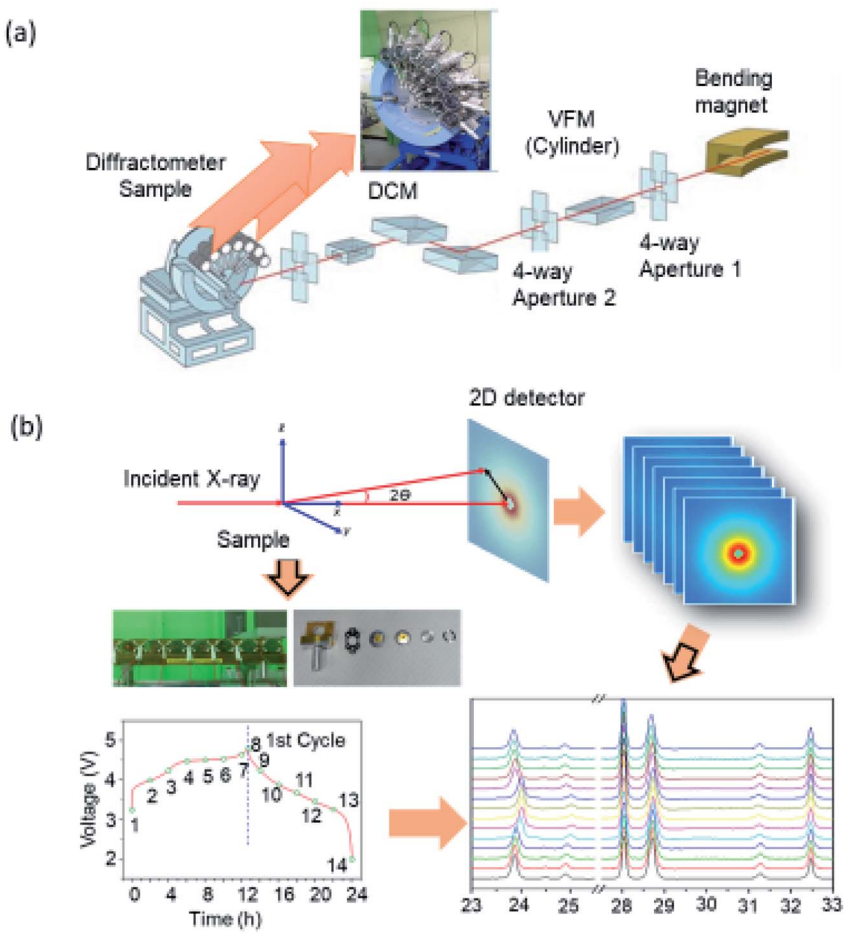

Fig. 4 (a) Optical layout of a typical high-resolution powder diffraction beamline along with multistage target holder. Adapted from https://pal.postech.ac.kr/bl/9B/(PLS)II. (b) Experimental procedure for performing *in situ* XRD along with the sample holder, electrochemical curve and HRPD patterns at various states of charging and discharging.

resolution powder diffraction (HRPD) beamline is shown in Fig. 4a.[128] The incident X-rays are vertically collimated by a mirror and monochromatized using a double-crystal Si(111) monochromator. The detector arm of the vertical scan diffractometer is composed of seven sets of Soller slits, flat Ge(111) crystal analyzers, anti-scatter baffles, and scintillation detectors, with each set separated by 20°. Fig. 4b shows the experimental procedure for *in situ* XRD of cathode. A coin-cell type battery with an electrode enabling measurement of XRD patterns at different stages of charging and discharging for the 1st cycle is designed. These patterns are recorded using a two-dimensional (2d) imaging plate and converted into a regular pattern by appropriate procedure.

The Rietveld refinement of the XRD pattern gives information of metal ion occupancy in the lattice of material under investigation.[131,132] Several methods[133,134] are developed to extract peak position, intensities, and width from XRD patterns for quantitative analysis of structural parameters. The most common powder XRD refinement technique is based on the method proposed in the 1960s by Hugo Rietveld.[135]

Fig. 5a shows the refined HRPD pattern of the $LiNi_{0.87}Co_{0.09}Mn_{0.04}O_2$ cathode using the Rietveld method. This pattern shows the presence of a layered structure. Estimated structural parameters are collated in Table 2. Due to better sensitivity, this technique is able to get insights into intermediate phases occurring during the growth of $LiNi_{1/3}Co_{1/3}Mn_{1/3}O_2$ cathode.[136] In addition to this, these measurements are able to depict the surface nature of cathode. Patterns obtained from synchrotron X-ray reveal presence of NiO-like rock-salt phase by the reconstruction of surfaces in water washed $LiNi_{0.88}Co_{0.054}Mn_{0.066}O_2$.[137]

This technique is used to establish the reversibility of crystallographic changes in NCM material during an electrochemical cycle.[138–140] Numerous reports are available showing the abrupt lattice collapse in the material during charging of LIB having Ni-rich cathode.[141–143] This phenomenon is ascribed to the Li utilization in the cathode material during charging and discharging by using *in situ* synchrotron X-ray diffraction.[144]

Table 2 Structural and refined parameters from Rietveld refinement of HRPD pattern

Space group				$R\bar{3}m$	
a (Å)/c (Å)				2.87402(2)/14.2018(1)	
Atom	Site	Wyckoff positions			Occupancy[a,c]
Li	3a	0	0	0	0.0812(2)
Ni2	3a	0	0	0	0.0021(2)
Ni1	3b	0	0	0.5	0.0703[b]
Co	3b	0	0	0.5	0.0075[b]
Mn	3b	0	0	0.5	0.0032[b]
O	6c	0	0	0.2419(1)	0.166[b]
Reliability factors		$R_p = 6.67\%$, $R_{wp} = 9.22\%$, $R_{exp} = 5.99\%$, $S = 1.54$			

[a] The normalized site occupation numbers in % are: Li1 : Ni2 (97.52 : 2.48), Ni1 : Co : Mn (84.48 : 8.99 : 3.88), O (100). [b] Fixed parameter. [c] The occupancy were achieved by using the constraints as follows. $Li_{3a} + Ni_{3a} = 0.08333$, $Mn_{3b} + Co_{3b} + Ni_{3b} + Ni_{3a} = 0.08333$.

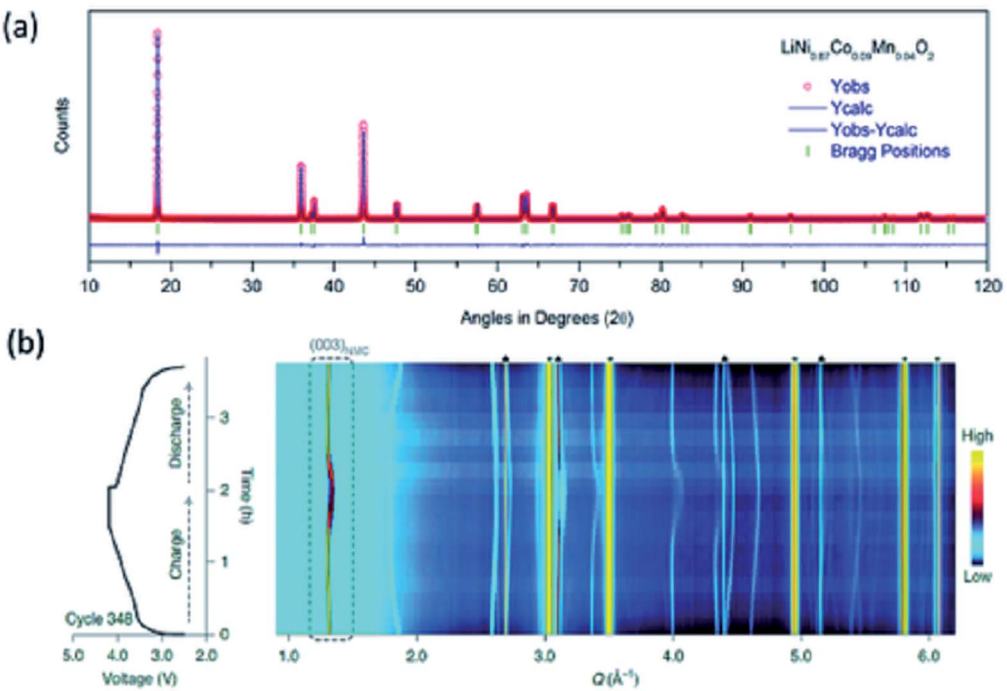

Fig. 5 (a) Refined HRPD pattern for $LiNi_{0.87}Co_{0.09}Mn_{0.04}O_2$ cathode material of LIB battery. (b) Voltage profile during cycle 348 of $LiNi_{0.8}Mn_{0.1}Co_{0.1}O_2$ and the corresponding diffraction patterns. The colour scale indicates the intensity of the diffraction signals in arbitrary units. Reproduced from ref. 155 with permission from [Springer Nature], copyright [2021].

The use of synchrotron X-ray is not only limited to structural phase identification and quantitative estimation of lattice constants but it is also explored to investigate phase transition in Li-rich layered $Li_{1.23}Ni_{0.09}Co_{0.12}Mn_{0.56}O_2$ during cycling,[145] $LiNi_{1/3}Mn_{1/3}Co_{1/3}O_2$ at various C-rates[146] and in $LiNi_{0.85}Co_{0.10}Mn_{0.05}O_2$.[147] This technique also gives information of metal ion occupancy in the lattice,[148,149] cation disorder[150–152] by suitable refinement procedure. By employing *in situ* methodology, it can track cationic ordering/disordering in Ni-rich cathode during electrochemical cycle.[153]

Fatigue phase formation during a long cycle has also been established by synchrotron X-ray.[154,155] In order to throw light on fatigue phase process, *in situ* X-ray study was reported by Xu *et al.*[155] Fig. 5c shows the phase segregation in polycrystalline $LiNi_{0.8}Mn_{0.1}Co_{0.1}O_2$ at a high state of charge (SoCs) at voltage profile during a particular cycle.[155] This is associated with fatigue phase formation induced by surface reconstructions.[156]

In situ heating XRD, which is also termed as time-resolved (TR) XRD is a unique technique for investigation of real-time structural changes in the material during heating.[157,158] Thus, it helps to understand the degradation and stability of cathode materials.[159–163] These measurements show that thermal stability of charged $LiNi_xMn_yCo_zO_2$ (NMC, with $x + y + z = 1$, $x : y : z = 4 : 3 : 3$ (NMC433), $5 : 3 : 2$ (NMC532), $6 : 2 : 2$ (NMC622), and $8 : 1 : 1$ (NMC811)) cathode decreases with increasing Ni content.[159] Using this technique, Lipson *et al.*, have shown that doping with Mg and Zr can impart substantial stabilization to Ni-rich cathode.[164]

Chemical/oxidation state investigation

X-rays have sufficient energy to eject a core electron from an atom. Each core–shell has distinct binding energy. When the X-ray energy is scanned through the binding energy of a core–shell, there is an abrupt increase in absorption cross-section (Fig. 6a).[165] This gives rise to a so-called absorption edge, with each edge representing a different core–electron binding energy. These edges are named according to the principle quantum number, n, of the electron that is excited (Fig. 6b). For example, K-edge for $n = 1$, L-edge for $n = 2$, M-edge for $n = 3$, *etc.*

The core-electron binding energy increases with increasing atomic number, ranging from 284 (C K-edge) to 115 606 eV (U K-edge).[166] Thus, XAS is the measurement of the binding energy of elements by scanning material through X-ray.

XAS can probe the local electronic/atomic structure, thereby depicts information on oxidation states and atomic coordination. Thus, it is suitable to investigate a complete account of the surroundings of the element under investigation.[167,168] These measurements, when performed for the X-ray energy up to 1000 eV from the main edge of element, are known as extended X-ray absorption fine structure (EXAFS) and are termed as X-ray absorption near edge fine structure (XANES) when performed in the energy range −20 to 60 eV from the main edge (Fig. 6c). The elements in the energy range of −20 to 60 eV from their edges can be probed either using hard X-ray or soft X-ray. However, measurement is often termed as XANES in the case of hard X-rays and near-edge X-ray absorption fine structure (NEXAFS) in the case of soft X-rays.

NEXAFS

Fig. 7a shows the optical layout of the soft-X-ray beamline having energy range of 200 to 1500 eV.[169] NEXAFS spectrum for a given material can be measured in either total electronic yield (TEY) or total fluorescence yield (TFY) modes along with the angle dependence depending upon the requirement

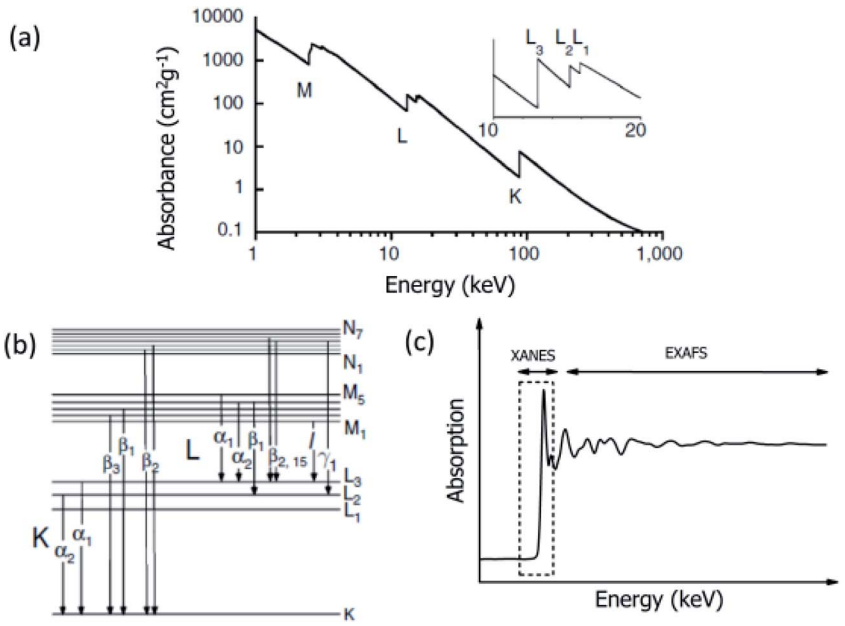

Fig. 6 (a) Absorbance as a function of energy. There is abrupt change in the absorbance corresponding to K, L and M shells. Inset (a) shows similar changes observed for L_1, L_2 and L_3 subshells. (b) Atomic energy levels showing electronic transitions corresponding to various shells. (c) A typical X-ray absorption spectrum showing the XANES and EXAFS regions.

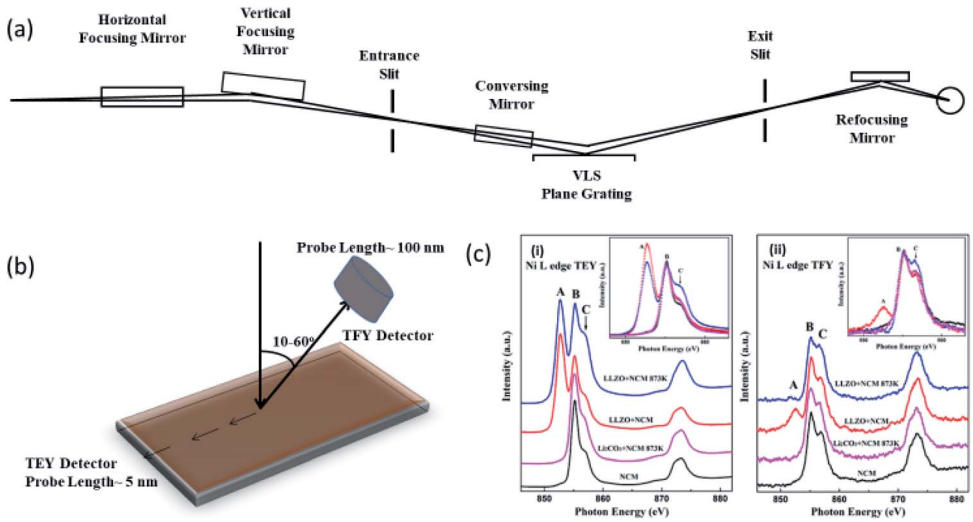

Fig. 7 (a) Optical lay-out of soft X-ray beamline. Reproduced from ref. 169 with permission from [Elsevier], copyright [2007]. (b) Schematic representation of TEY and TFY mode; (c) NEXAFS spectra of NCM cathodes attached to LLZO and $LiCoO_2$ cathodes. Reproduced from ref. 174 with permission from [ACS], copyright [2018].

(Fig. 7b).[170,171] TEY measurements probe the surface of materials (~5 nm),[172] however, depth is probed using TFY counterpart (50-100 nm).[173] Fig. 7c shows the Ni L-edge NEXAFS spectra in TEY (i) and TFY mode (ii) for NCM attached with $Li_7La_3Zr_2O_{12}$ (LLZO) and Li_2CoO_2.[174] These measurements reflect significant changes on the surface and bulk of this cathode.

EXAFS

Fig. 8a depicts the schematic of beamline for measuring hard XAS.[175] Experimental end station of this beamline is shown in Fig. 8b which exhibits the feasibility of performing measurements in both transmission and fluorescence mode. With a suitable experimental arrangement, coin cell can be studied during an electrochemical reaction (Fig. 8c).[176] Thus, this beamline provides facility to probe cathodes either *in situ*[176] or *ex situ* mode.[177] Fig. 8d shows the Mn K-edge XAS spectra of Li_2MnSO_4 cathode at different charging and discharging states along with Mn oxide references.[178]

Both the NEXAFS and XANES measurements can give information on the oxidation state of constituent ions of cathodes.[179] The oxidation state of Mn ions in $LiMn_2O_4$ is determined by comparing it's XANES spectra with that of Mn_2O_3 and MnO_2. Mn ions have a 3.5 valence state in this cathode (Fig. 9a).[180] These measurements show that Mn^{3+} oxidation state is a mixture of the high spin (HS) and low spin (LS) states in $LiMnO_2$ cathode.[181] The exact information of Mn oxidation state

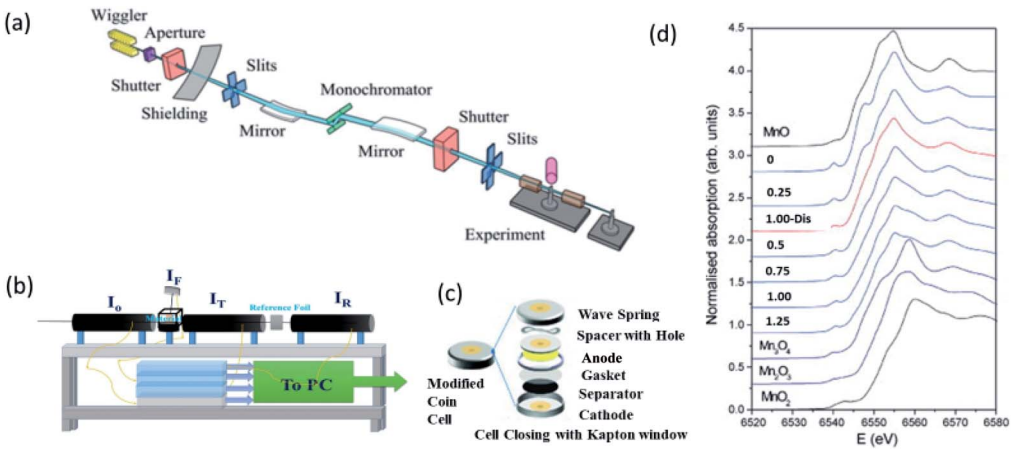

Fig. 8 (a) Schematic of bending magnetic based XAS beamline. Reproduced from ref. 173 with permission from [AIP Publishing], copyright [2010]. (b) Representative end station for measuring XAS spectrum. (c) Schematic of coin cell used for *in situ* XAS measurements of cathode materials. Reproduced from ref. 176 with permission from [Springer Nature], copyright [2018]. (d) Mn K-edge XAS spectra of $Li_{2-x}MnSO_4$ cathode at different charging ($x = 0.0$–1.25) and discharging ($x = 1.0$-dis) states along with Mn oxides. Reproduced from ref. 178 with permission from [Elsevier], copyright [2008].

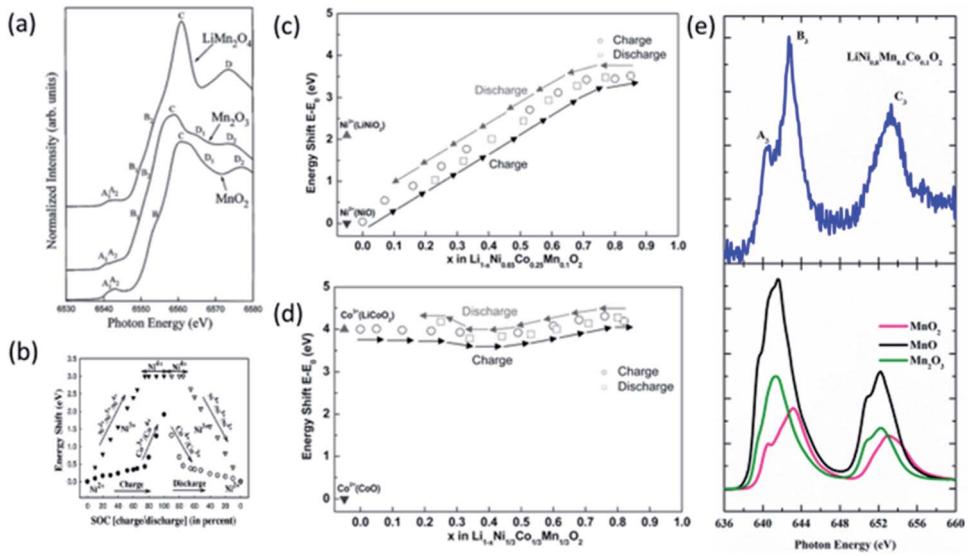

Fig. 9 (a) Mn K-edge XANES spectra of $LiMn_2O_4$ cathode material along with reference oxides, MnO, Mn_2O_3 and MnO_2. Reproduced from ref. 180 with permission from [Elsevier], copyright [1997]. (b) Plot of the white line energy shift *vs.* the state of charge (SOC) for Co and Ni K edge. The filled symbols represent the data during charging (*i.e.* during delithiation), while the empty symbols represent the data during discharging (*i.e.* during lithiation). Reproduced from ref. 183 with permission from [AIP publishing], copyright [2005]; energy shift $E-E_0$ of the (c) Co K-edge and (d) Ni K-edge at the half-height of the edge step for $Li_{1-x}Ni_{1/3}Co_{1/3}Mn_{1/3}O_2$ at different lithium concentration during first charge and discharge cycle. Reproduced from ref. 189 with permission from [ACS], copyright [2005]. (e) Mn L-edge NEXAFS spectrum of $LiNi_{0.8}Mn_{0.1}O_{0.1}$ cathode material along with Mn oxides.

in $LiMn_2O_4$ is carried out by plotting half-height energy values for the reference compound. The procedure of determining the oxidation state of unknown compound is depicted in Section S1.† This estimates the valence state of Mn at the fully discharged state to be approximately 3.6+.[182]

XANES studies show that the oxidation state of Ni, Mn, and Co ions are 2+, 4+, and 3+ in the NCM333 cathode.[183] These estimated oxidation states are in line with that determined from X-ray photoelectron spectroscopy.[184,185] This material depicts the change of oxidation state of Ni and Co ions from the energy shift of the white line (Section S1†) during the charging and discharging of cathode (Fig. 9b).[183] Similar observations were carried out by Tian *et al.* for $LiNi_{0.6}Mn_{0.2}Co_{0.2}O_2$ using XAS[186] and from soft *X*-ray spectroscopy.[187] *In situ* hard XAS exhibits no change of Mn oxidation state during the de-lithiation and lithiation for $LiNi_{0.6}Mn_{0.2}Co_{0.2}O_2$ cathode. These measurements show systematic changes are observed for Ni and Co ions.[188] This effect is associated with migration and insertion of Li ions into the NCM cathode as Ni oxidation state is sensitive to the Li content (Fig. 9c), however, it's influence is almost non-significant on the oxidation state of Co ions (Fig. 9d).[189]

Apart from the XANES measurements, NEXAFS is also helpful to get quantitative information on mixed oxidation states.[190] Authors have reported the presence of mixed Fe^{2+} and Fe^{3+} oxidation states of Fe ions in Li_xFePO_4 cathode material;[191] Mn^{3+}, and Mn^{4+} in $Na_{0.44}MnO_2$ electrode[192] from these measurements. Mn K-edge NEXAFS spectrum of NCM811 along with MnO, Mn_2O_3, and MnO_2 is shown in Fig. 9e. The spectral features A_3, B_3, and C_3 are analogs to that observed for MnO_2, revealing the 4+ oxidation.

In addition to depict the information of oxidation state *via* metal L-edge, NEXAFS also give information of M–O hybridization process from the O K-edge measurements. Information on this aspect can be revealed by analyzing the pre-edge region of the O K-edge spectrum of cathode.[193–195] Our group has investigated this effect in NCM811 cathode using O K-edge NEXAFS during the charging and discharging.[188] Since, in layered oxides, metal–oxygen bond is important for oxygen-redox activity,[189,190] hence, information specific to M–O hybridization is very effective to gather information of this activity.[196] Koo *et al.* explain the redox mechanism of both cationic and anionic activity across the full cycling range of NCM333 materials by determining M–O hybridization from the pre-edge region of O K-edge.[197] Thus, these measurements persist a way to throw light on the redox mechanism in these cathodes.[198,199]

Local atomic structure investigation

EXAFS spectrum of material gives quantitative information of coordination number (N) and bond-lengths (R) using proper simulation process.[200–202] VIPER,[203] LARCH,[204] EVAX[205] and Demeter[206] are the data processing package used for simulation purposes. A typical equation for the EXAFS, which is basis for simulation is given below

$$\chi(k) = \sum_z \frac{N_z S_0^2 f_z(k)}{kR_z^2} e^{2k^2\sigma_z^2} e^{-\frac{2R_z}{\lambda_z(k)}} \sin[2kR_z + \delta_z(k)] \quad (1)$$

where N_z is the total number of atoms in the z^{th} shell, λ is the mean free path of photoelectron, and f_z is the backscattering amplitude. The term before sin function represents the

Table 3 Parameters and their criteria for EXAFS simulation

Parameters	Representation	Origin	Fitting criteria	Characteristics	Determination
S_0^2	Amplitude reduction factor	Intrinsic losses due to inelastic effects in the EXAFS equation	$0.7 < S_0^2 < 1.0$	Remains same for similar structure	From the standard
N	Degeneracy	Coordination number of known atomic species		Depends on the structure	
ΔR	Change in bond-length	Bond-length among atomic species	≤ 0.05		Determined independently for each path
ΔE_0	Correction to main edge	Uncertainty in determination of energy E_0	≤ 2		One value for the energy shift (E_0) can be applied to all paths
σ^2	Mean-squared displacement of the half path length	The thermal and static disorders are similar in the coordination shells	≤ 0.003		

amplitude of the wave, which can be explained using the following equation,

$$A_z(k) = \sum_z \frac{N_z S_0^2 f_z(k)}{kR_z^2} e^{2k^2\sigma_z^2} e^{-\frac{2R_z}{\lambda_z(k)}} \quad (2)$$

In eqn (2), σ represents a fluctuation in R_z due to structural disorder and temperature. The part sin $[2kR_z + \delta_z(k)]$ of the EXAFS equation represents the oscillation. The term $\delta_z(k)$ is the phase shift. The EXAFS equation represents it's dependence on the number of atoms in a particular shell, bond distance R_z, scattering amplitude. Thus, proper adjustment of scattering amplitude and disorder term, S, enables one to determine the number of atoms and bond distance, which is done by simulating the EXAFS spectrum using a particular program.[207,208] The parameters given in Table 3 need specific consideration during simulation.[209,210] Thus, criteria for simulation of EXAFS spectrum[210–212] can provide precise bond-length[160,161] and coordination number of shells.[213]

Fig. 10 shows the results obtained from XAS study of $0.5Li_2MnO_3 \cdot 0.5LiCoO_2$, $Li[Ni_{0.17}Li_{0.2}Co_{0.07}Mn_{0.56}]O_2$ and NCM333 cathodes.[214,215] XANES spectra and k^2-weighted Fourier-transformed EXAFS signals at the Mn and Co K-edges of the $0.5Li_2MnO_3 \cdot 0.5LiCoO_2$ synthesized using ball-milling and sol–gel method are shown in Fig. 10a and b. The XANES spectra at Mn and Co edges almost overlap for both synthesis methods showing presence of these atoms in similar environments with quite similar local structures.

To get deeper insights of local atomic structure, these authors have also compared the Fourier transform of EXAFS spectra and observed significant changes in the peak corresponding to Mn/Co–M bonds. These differences in EXAFS spectra due to the different Li_2MnO_3 and $LiCoO_2$ domain sizes, indicating different phase separation behaviors. In another experiment carried out for $Li[Ni_{0.17}Li_{0.2}Co_{0.07}Mn_{0.56}]O_2$ and NCM333, authors observed differences in the peak corresponding to M–O shell with dominant effect corresponding to Mn–O shell. This is associated with the difference in surrounding of Mn sites in both oxides. Quantitative information of local atomic structure revealed by simulation of EXAFS spectra is collated in Table 4.

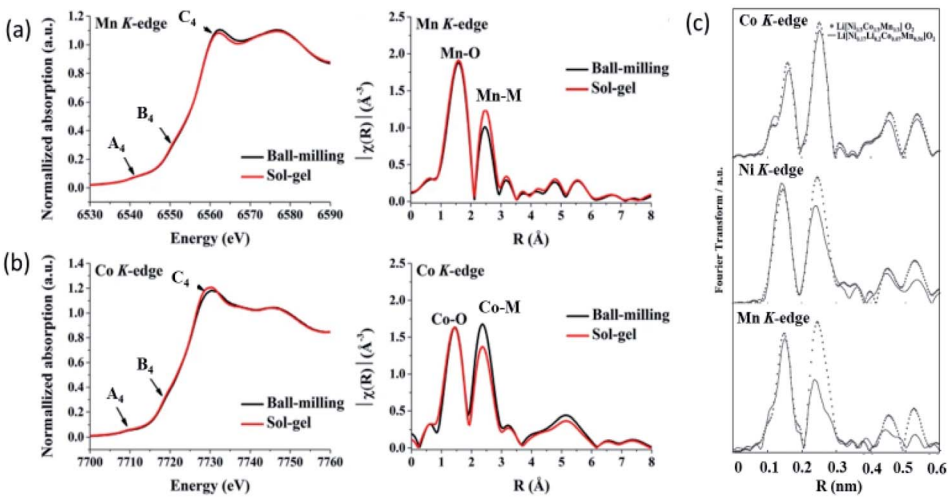

Fig. 10 XANES spectra and k^2-weighted Fourier-transformed EXAFS signals at the (a) Mn and (b) Co K-edges of the $0.5Li_2MnO_3 \cdot 0.5LiCoO_2$ materials. Reproduced from ref. 214 with permission from [Springer Nature], copyright [2019]. (c) k^3-Weighted Fourier transforms for Ni, Co, and Mn absorbers for $Li[Ni_{0.17}Li_{0.2}Co_{0.07}Mn_{0.56}]O_2$ and $Li[Ni_{1/3}Co_{1/3}Mn_{1/3}]O_2$. Reproduced from ref. 215 with permission from [The Electrochemical Society of Japan], copyright [2010].

Table 4 Co-ordination number (N). Bond-distance (R), Debye–Waller factor (σ^2) for different materials estimated from Ni K-edge spectra. Reproduced from ref. 215 with permission from [The Electrochemical Society of Japan], copyright [2010]

	Shell	N	R (Å)			
Materials	Ni–O	Co–O	Mn–O	σ^2 (Å^2) (10^{-5} nm^2)	N	Fitting range (nm^{-1})
$Li[Ni_{0.17}Li_{0.2}Co_{0.07}Mn_{0.56}]O_2$	0.02023 ± 0.0011			5.1	6	$20 < k < 120$
		0.1918 ± 0.0012		3.7	6	$26 < k < 107$
			0.1913 ± 0.0010	2.6	6	$27.5 < k < 119$
$Li[Ni_{1/3}Co_{1/3}Mn_{1/3}]O_2$	0.02020 ± 0.0010			3.8	6	$20 < k < 120$
		0.1910 ± 0.0012		2.2	6	$26 < k < 107$
			0.1922 ± 0.0011	3.1	6	$27.5 < k < 119$
$LiNiO_2$	0.197			12.1	6	$27 < k < 118$
$LiCoO_2$		0.193		3.0	6	$27 < k < 121$
$LiMnO_2$			0.192	2.3	6	$27.5 < k < 120$

Tsai *et al.* quantitatively investigated the M (Ni, Mn, & Co)–O and M–M bond lengths in NCM333 cathode using EXAFS studies during cycling. Reduction of bond-lengths with the increase of Li-ion concentration is reported by this group.[189] M–O bond-lengths in $Li[Ni_{0.17}Li_{0.2}Co_{0.07}Mn_{0.56}]O_2$ cathode material decrease upon charging and retains values equivalent to original after discharging.[182] These studies are carried out to investigate the modulation of both CNs and bond-length of Ni–O and Ni-metal during charging, discharging for NCM333 cathode during various stages of charging and discharging.[183]

XAS also gives information of vacancies in cathode materials of LIB.[216,217] These kinds of investigations give understanding of the degradation mechanisms in NCM cathode materials.[218,219] Using this technique, Lee *et al.* reported that the formation of oxygen vacancies around Ni could be inferred to be more pronounced in a cathode material with a higher Ni content.[220]

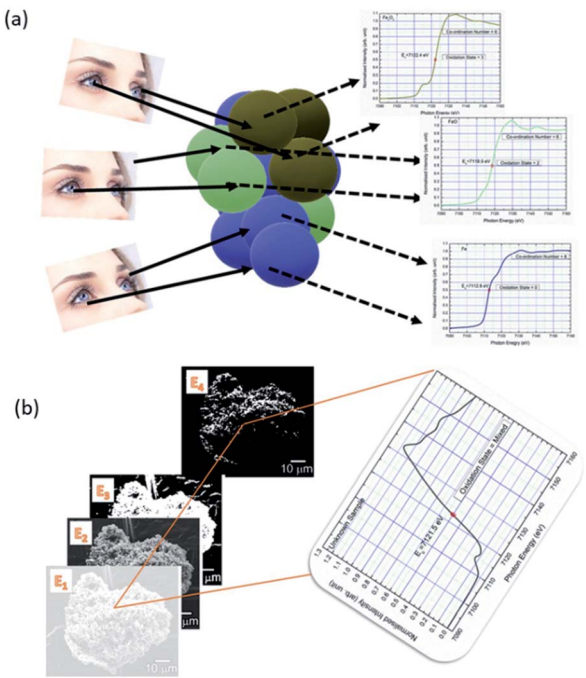

Fig. 11 (a) Schematic representation of visualization of regions of different oxidation states in materials. (b) Principle of obtaining of XANES spectrum from X-ray imaging.

Chemical phase mapping

Chemical phase mapping is the process of visualizing the regions of different oxidation states in a particular material by measuring XANES spectra (Fig. 11a). Technique to obtain this mapping is known as XANES-imaging. In this technique, multiple 2d images of material are produced to obtain spatially resolved information.[221–223] Fig. 11b illustrates the change of intensity distribution for 2d images with a change of X-ray energy (Fig. 11b). Thus, pixel counts as a function of X-ray energy forms the XANES spectrum of the element in the material.

In this experiment, a set of raw data obtained from 2d imaging XAS measurement consists of a 3d array of the transmitted X-ray intensities, $I(E'(x,y))$, where, E' is the apparent X-ray energy and (x,y) is the measurement position on the sample.[224]

The X-ray absorbance, μt at each position (x,y) is expressed by the following equation,

$$\mu t(E',x,y) = \ln[I_0(E',x,y)/I(E',x,y)] \quad (3)$$

where, the ionization chamber measures the incident X-ray intensities, the $I_0(E',x,y)$ term is replaced by the detected value at E'. The spectrum for a specific area can be obtained by integrating $\mu t(E',x,y)$.

To get the XANES-imaging spectrum, the samples are mounted on a platform placed between the incident X-ray and charged coupled device (CCD) detector, as shown in Fig. 12a. Sample images (Fig. 12b) along with background images (Fig. 12c) at different X-ray energies are recorded using a CCD.[225] After obtaining various images, each image at specific X-ray energy is corrected with respect to the background. These images are aligned and converted into the XANES spectrum. After obtaining, spectrum, chemical speciation of the material is performed using linear combination fitting (LCF).

Thus, XANES-imaging experiments are performed along with appropriate references to get chemical phase mapping of

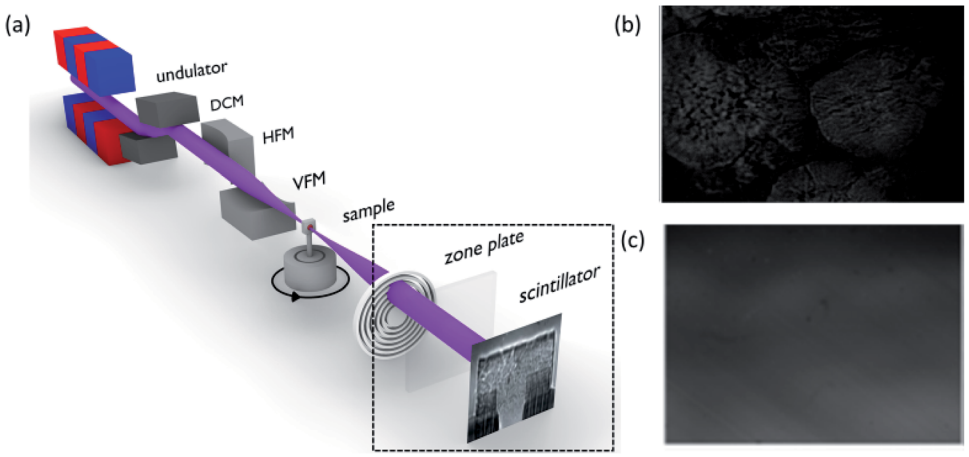

Fig. 12 (a) Schematic of a typical X-ray-imaging beamline for XANES measurements. DCM-double crystal monitor, HFM-horizontal focusing mirror, VFM-vertical focusing mirror. Reproduced from ref. 225 with permission from [IUCr], copyright [2020]. (b) X-ray image measured for NCM111 cathode material and (c) background image.

material. Schematic of obtaining chemical phase mapping is given as ESI (Section S2†).

This technique is considered suitable for determining chemical phase mapping at various states of charging and discharging. 2d-XANES imaging applied to $LiFePO_4$ cathode material of Li-battery shows that both the $LiFePO_4$ and $FePO_4$ phase co-exists during charging.[226] In another work, this technique is applied to NCM622 cathode (Fig. 13a)[227] and to visualize the Ni oxidation state distribution in radially aligned grains and randomly oriented grains-NCM.[228] Fig. 13(a) shows that a near-complete phase transition occurs at the final charge and discharge stage, indicating highly electrochemical reversibility in case of NCM622. Nevertheless, high reversibility cannot survive after 200 cycles, which is unambiguously revealed through *operando* transmission X-ray microscopy (TXM) chemical phase mapping. During the 201st charge cycle a highly heterogeneous chemical phase distribution appears in single-crystal NCM (Fig. 13a).[228]

In a recent study from our group,[229] this technique is effectively applied to visualize the chemical distribution map of the discharged cathode at a charging rate of 3C. The results are shown in Fig. 13b. The results also exhibit the reversibility of chemical phase after comparison of pristine (i), charged (ii) and discharged NCM333 cathode (ii).

Tomography

X-ray imaging is well established to quantify the deformation of a single secondary particle, and its detailed investigation is discussed by Liu *et al.* for NCM cathode.[230,231] Experimental

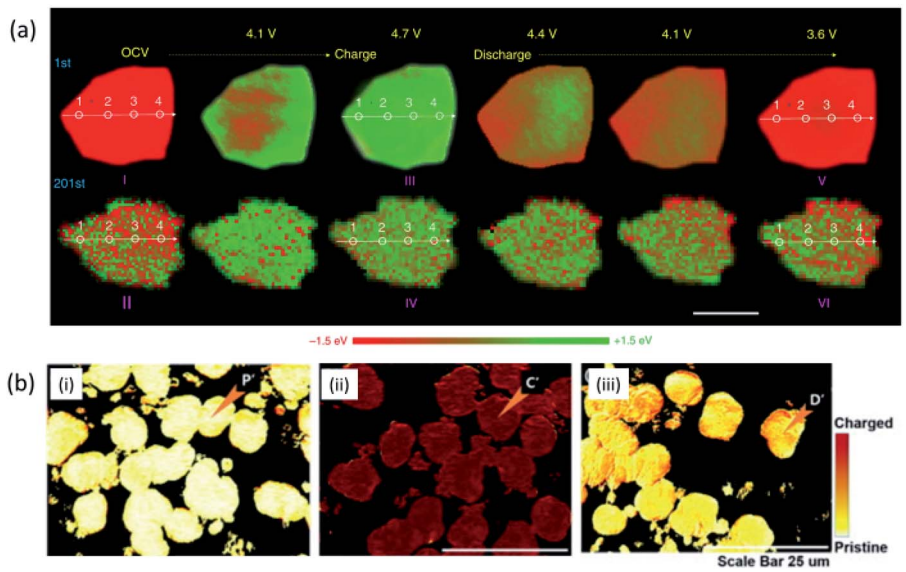

Fig. 13 (a) *Operando* 2D chemical phase mappings at the Ni K-edge of NCM particles during the first and 201st cycles. Scale bars 2 μm. Reproduced from ref. 227 with permission from [Springer Nature], copyright [2020]. (b) XANES-mapping of pristine, charged and discharged cathode materials. Reproduced from ref. 229 with permission from [Elsevier], copyright [2020].

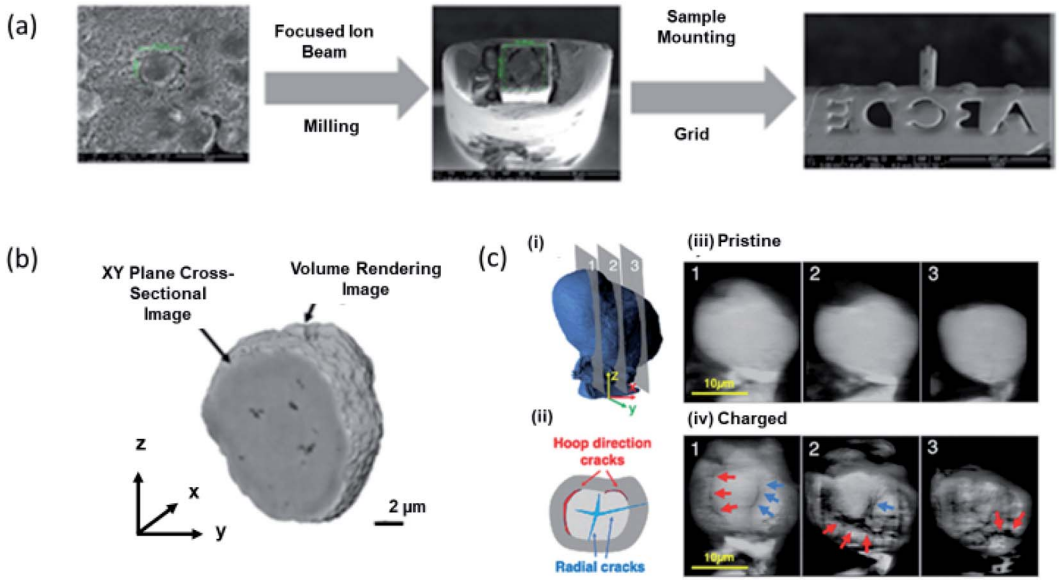

Fig. 14 (a) Sample preparation for X-ray tomographic measurements. (b) X-ray tomographic image of $LiNi_{0.8}Co_{0.1}Mn_{0.1}O_2$ cathode. (c) (i) 3D ptycho-tomography reconstruction of a single particle in a pristine state with an indication of cross-sectional planes 1–3 shown on the right. (ii) Reconstructed ptychography slices of pristine single particle. (iii) Crack types observed after single charge: cracks in radial direction initiated in the core (blue) and cracks in hoop direction along core–shell interface (red). (iv) Reconstructed ptychography slices after a single charge up to 17.8% SoC, revealing significant microstructural degradation in radial direction (blue arrows) and along the core–shell interface (red). Reproduced from ref. 232 with permission from [RSC], copyright [2020].

procedure and tomographic images obtained for $LiNi_{0.8}Co_{0.1}Mn_{0.1}O_2$ cathode are shown in Fig. 14a (Section S3†). These measurements revealed almost 1.85% porosity of the secondary particle (Fig. 14b). Sub-micron focused *operando* synchrotron XRD and *in situ* ptycho-tomographic nano-scale imaging of a single nano-structured $LiNi_{0.8}Co_{0.1}Mn_{0.1}O_2$ core–shell particle during charge gives a thorough understanding of the anisotropic deformation and damage phenomena at a particle level (Fig. 14c).[232]

Thus, these techniques are very effective in probing the cathode materials of LIB, and numerous researchers carefully review their effectiveness with a combined approach to understand the degradation mechanism by looking into structure, local atomic structure, chemical phase mapping and tomography of the cathode.[233–235] However, there is a rare use of these techniques in combined way. Our group recently investigated by combining these techniques that first cycle irreversibility is associated with the irreversibility of Ni oxidation states. Chemical state irreversibility of Ni ions is affected by the pore distribution in the cathode. During the first cycle, both the local structure and long-range structure remain unaltered.[236] Thus, we believe that cumulative applications of these characterization techniques will be able to solve various issues of LIB. Since, still there are numerous challenges to exactly identifying the structural behaviour of NCM cathode surface, hence, the techniques such as single-shot coherent X-ray imaging[237] and transient X-ray absorption spectroscopy[238,239] developed at 4th generation synchrotron facility may be effective.[240] However, the use of these techniques for battery research are in infant stages till date.

Conclusions

This review paper briefly describes Li-ion rechargeable batteries and related synchrotron techniques. A description of the phenomena that can be investigated using these techniques is also discussed in a concise way. XRD that determines long-range structure order is also helpful to throw light on the thermal stability of cathodes by temperature dependent measurements. This technique depicts the fatigue process in cathodes. XAS gives information on oxidation state and local atomic structure of cathode materials. It is also suitable to investigate the metal–oxygen hybridization process as well as oxygen vacancies in the cathodes. XANES-imaging visualizes the distribution of the chemical state on the particle surface. X-ray imaging provides tomographic information of particles of cathodes. It can also analyze cracks and pores quantitatively. Thus, synchrotron radiation analytical tools are effective to give a complete overview of the NCM cathodes during charging and discharging of LIB by their structure, local electronic/atomic structure, chemical phase mapping and tomography.

Author contributions

JPS, and SL conceptualise the idea. JPS wrote the manuscript in consultation with KHC, DA and SL. AKP revised the manuscript. SL and DA supervise the work. All authors have approved the manuscript.

Conflicts of interest

There are no conflicts to declare.

Acknowledgements

This research was supported by Commercializations Promotion Agency for R&D Outcomes (COMPA) funded by the Ministry of Science and ICT (1711149965). This work was also supported by Korea Institute of Science and Technology (KIST Project No. 2V09190). D. Ahn acknowledges financial supporting of the National Research Foundation of Korea (NRF) funded by the MSIT (2021M3H4A1A02049904) and Technology Innovation Program (Alchemist Project, 20012196, Al based supercritical materials discovery) funded by the Ministry of Trade, Industry & Energy, Korea. JPS acknowledges Science and Engineering Research Board, Department of Science and Technology, New Delhi, India for providing research grant through Ramanujan Fellowship (RJF2021/000115).

Notes and references

1 H. Sun, Y. Zhang, J. Zhang, X. Sun and H. Peng, *Nat. Rev. Mater.*, 2017, **2**, 17023.
2 S. Staffell, D. Scamman, A. V. Abad, P. Balcombe, P. E. Dodds, P. Ekins, N. Shah and K. R. Ward, *Energy Environ. Sci.*, 2019, **12**, 463.
3 T. Liu, Y. Zhang, Z. Jiang, X. Zeng, J. Ji, Z. Li, X. Gao, M. Sun, Z. Lin, M. Ling, J. Zheng and C. Liang, *Energy Environ. Sci.*, 2019, **12**, 1512.
4 Q. Liu, Z. Hu, W. Li, C. Zhou, H. Jin, S. Wang, S. Chou and S. X. Dou, *Energy Environ. Sci.*, 2021, **14**, 158.
5 A. Noori, M. F. El-Kady, M. S. Rahmanifar, R. B. Kaner and M. F. Mousavi, *Chem. Soc. Rev.*, 2019, **48**, 1272.
6 K. Schmidt-Rohr, *J. Chem. Educ.*, 2018, **95**, 1801.
7 G. J. May, A. Davidson and B. Monahov, *J. Energy Storage*, 2018, **15**, 145.
8 M. G. Choi, K. M. Kim and Y.-Gi Lee, *Curr. Appl. Phys.*, 2010, **10**, e92.
9 X. Chen, X. Liu, Q. Le, M. Zhang, M. Liu and A. Atrens, *J. Mater. Chem. A*, 2021, **9**, 12367.
10 G. Blomgren, Primary Batteries, Selection and Application, in *Encyclopedia of Applied Electrochemistry*, ed. G. Kreysa, K. Ota and R. F. Savinell, Springer, New York, NY, 2014, DOI: 10.1007/978-1-4419-6996-5_387.
11 H. Wang, X. Liang, J. Wang, S. Jiao and D. Xue, *Nanoscale*, 2020, **12**, 14.
12 M. Winter, B. Barnett and K. Xu, *Chem. Rev.*, 2018, **118**, 11433.
13 W. Chen, J. Liang, Z. Yang and G. Li, *Energy Procedia*, 2019, **158**, 4363.
14 Y. Liang, C.-Z. Zhao, H. Yuan, Y. Chen, W. Zhang, J.-Q. Huang, D. Yu, Y. Liu, M.-M. Titirici, Yu-L. Chueh, H. Yu and Q. Zhang, *InfoMat*, 2019, **1**, 6.
15 C. P. Grey and D. S. Hall, *Nat. Commun.*, 2020, **11**, 6279.
16 F. Wu, J. Maier and Y. Yu, *Chem. Soc. Rev.*, 2020, **49**, 1569.
17 M. Rosa Palacin, *Acc. Mater. Res.*, 2021, **2**, 319.
18 D. E. Eapen, R. Suresh, S. Patil and R. Rengaswamy, *Renewable Sustainable Energy Rev.*, 2021, **147**, 111165.
19 T. Chen, Y. Jin, H. Lv, A. Yang, M. Liu, B. Chen, Y. Xie and Q. Chen, *Trans. Tianjin Univ.*, 2020, **26**, 208.
20 M. Kwiecien, P. Schröer, M. Kuipers and D. U. Sauer, Current research topics for lead–acid batteries, in *Lead-acid batteries for future automobiles*, ed. J. Garche, E. Karden and D. A. J. Rand, 2017, p. 133.
21 K. Huang, J. Li and Z. Xu, *Waste Manag.*, 2010, **30**, 2292.
22 S. K. Dhar, S. R. Ovshínsky, P. R. Gifford, D. A. Corrigan, M. A. Fetcenko and S. Venkatesan, *J. Power Sources*, 1997, **65**, 1.
23 H.-L. Chen, P.-S. Wu and J.-J. Wu, *ACS Sustainable Chem. Eng.*, 2019, **20**, 17100.
24 B. Ji-Hoon, K. Sangwan, G. H. Dong and J.-C. Lee, *ACS Appl. Mater. Interfaces*, 2019, **11**, 29718.
25 A. Masias, J. Marcicki and W. A. Paxton, *ACS Energy Lett.*, 2021, **6**, 621.
26 J. Chidiac, L. Timperman and M. Anouti, *J. Energy Chem.*, 2022, **65**, 352.
27 J. Jiang, G. Nie and P. Nie, *Nano-Micro Lett.*, 2020, **12**, 183.
28 G. Zhu, X. Tian, H.-C. Tai, Y.-Y. Li, J. Li, H. Sun, P. Liang, M. Angell, C.-L. Huang, C.-S. Ku, W.-H. Hung, S.-K. Jiang, Y. Meng, H. Chen, M.-C. Lin, B.-. Hwang and H. Dai, *Nature*, 2021, **596**, 525.
29 J. W. Choi and D. Aurbach, *Nat. Rev. Mater.*, 2016, **1**, 16013.
30 R. Zhou, S. Wei, Y. Liu, N. Gao, G. Wang, J. Lian and Q. Jiang, *Sci. Rep.*, 2019, **9**, 3980.
31 B. D. McCloskey, *J. Phys. Chem. Lett.*, 2015, **6**, 18.
32 J.-M. Tarascon and M. Armand, *Nature*, 2001, **414**, 359.
33 R. Schmuch, R. Wagner, G. Hörpel, T. Placke and M. Winter, *Nat. Energy*, 2018, **3**, 267.
34 W. Zuo, M. Luo, X. Liu, J. Wu, H. Liu, J. Li, M. Winter, R. Fu, W. Yang and Y. Yang, *Energy Environ. Sci.*, 2020, **13**, 4450.
35 J. Xu, S. Dou, H. Liu and L. Dai, *Nanoenergy*, 2013, **2**, 439.
36 N. Nitta, F. Wu, J. T. Lee and G. Yushin, *Mater. Today*, 2015, **18**, 252.
37 N. Yabuuchia, M. Takeuchi, M. Nakayama, H. Shiiba, M. Ogawa, K. Nakayama, T. Ohta, D. Endo, T. Ozaki, T. Inamasu, K. Sato and S. Komab, *Proc. Natl. Acad. Sci. U. S. A.*, 2015, **112**, 7650.
38 T. Kim, W. Song, D.-Y. Son, L. K. Ono and Y. Qi, *J. Mater. Chem. A*, 2019, **7**, 2942.
39 T. M. Güra, *Energy Environ. Sci.*, 2018, **11**, 2696.
40 X. Fan, B. Liu, J. Liu, J. Ding, X. Han, Y. Deng, X. Lv, Y. Xie, B. Chen, W. Hu and C. Zhong, *Trans. Tianjin Univ.*, 2020, **26**, 92.
41 M. Li, J. Lu, Z. Chen and K. Amine, *Adv. Mater.*, 2018, **30**, 1800561.
42 B. L. Ellis, K. T. Lee and L. F. Nazar, *Chem. Mater.*, 2010, **22**, 691.
43 U.-H. Kim, D.-W. Jun, K.-J. Park, Q. Zhang, P. Kaghazchi, D. Aurbach, D. T. Major, G. Goobes, M. Dixit, N. Leifer, C. M. Wang, P. Yan, D. Ahn, K.-H. Kim, C. S. Yoon and Y.-K. Sun, *Energy Environ. Sci.*, 2018, **11**, 1271.
44 A. Mishra, A. Mehta, S. B. Shweta, J. Malode, N. P. Shetti, S. S. Shukla, M. N. Nadagouda and T. M. Aminabhavi, *Mater. Sci. Energy Technol.*, 2018, **1**, 182.
45 P. Roy and S. K. Srivastava, *J. Mater. Chem. A*, 2015, **3**, 2454.
46 Q. Zhang, Q.-F. Dongz, M.-S. Zheng and Z.-W. Tian, *J. Electrochem. Soc.*, 2011, **158**, A443.

47 W. Xu, J. Wang, F. Ding, X. Chen, E. Nasybulin, Y. Zhang and J.-G. Zhang, *Energy Environ. Sci.*, 2014, **7**, 513.
48 S. Tardif, E. Pavlenko, L. Quazuguel, M. Boniface, M. Maréchal, J.-S. Micha, L. Gonon, V. Mareau, G. Gebel, P. B. Guillemaud, F. Rieutord and S. Lyonnard, *ACS Nano*, 2017, **11**, 11306.
49 H. Aziam, G. Garhi, Y. Tamraoui, L. Ma, T. Wu, G. L. Xu, B. Manoun, J. Alami, K. Amine and I. Saadoune, *Electrochim. Acta*, 2018, **283**, 1238.
50 H. Aziam, S. Indris, H. B. Youcef, R. Witte, A. Sarapulova, H. Ehrenberg and I. Saadoune, *J. Alloys Compd.*, 2022, **906**, 164373.
51 C. Liu, Z. G. Neale and G. Cao, *Mater. Today*, 2016, **19**, 109.
52 W. Tang, G. Zhou, J. Cao, Z. Chen, Z. Yang, H. Huang, Y. Qu, C. Li, W. Zhang and H. Liu, *ACS Appl. Energy Mater.*, 2021, **4**, 2962.
53 F. Wu and G. Yusin, *Energy Environ. Sci.*, 2017, **10**, 435.
54 R. Chen, T. Zhao, X. Zhang, L. Li and F. Wu, *Nanoscale Horiz.*, 2016, **1**, 423.
55 H. Sun, J. Zhu, D. Baumann, L. Peng, Y. Xu, I. Shakir, Y. Huang and X. Duan, *Nat. Rev. Mater.*, 2019, **4**, 45.
56 F. Yang, D. Wang, Y. Xing and K.-L. Tsui, *Microelectron. Reliab.*, 2017, **70**, 70.
57 S.-T. Myung, F. Maglia, K.-J. Park, C. S. Yoon, P. Lamp, S.-J. Kim and Y.-K. Sun, *ACS Energy Lett.*, 2017, **2**, 196.
58 G. Che, K. B. Jirage, E. R. Fisher, C. R. Martin and H. Yoneyama, *J. Electrochem. Soc.*, 1997, **144**, 4296.
59 J. Cho, Y. W. Kim, B. Kim, J. G. Lee and B. Park, *Angew. Chem., Int. Ed.*, 2003, **42**, 1618.
60 T. Ohzuku, A. Ueda and M. Nagayama, *J. Electrochem. Soc.*, 1993, **140**, 1862.
61 P. Bruce, A. R. Armstrong and R. L. Gitzendanner, *J. Mater. Chem.*, 1999, **9**, 193.
62 F. Lin, I. M. Markus, D. Nordlund, T.-C. Weng, M. D. Asta, H. L. Xin and M. M. Doeff, *Nat. Commun.*, 2014, **5**, 3529.
63 S. K. Martha, O. Haik, E. Zinigrad, I. Exnar, T. Drezen, J. H. Miners and D. Aurbach, *J. Electrochem. Soc.*, 2011, **158**, A1115.
64 R. Wang, X. He, L. He, F. Wang, R. Xiao, L. Gu, H. Li and L. Chen, *Adv. Energy Mater.*, 2013, **3**, 1358.
65 M.-J. Lee, S. Lee, P. Oh, Y. Kim and J. Cho, *Nano Lett.*, 2014, **14**, 993.
66 S. Choi and A. Manthiram, *J. Electrochem. Soc.*, 2002, **149**, A162.
67 A. Yamada, S. C. Chung and K. Hinokuma, *J. Electrochem. Soc.*, 2001, **148**, A224.
68 D. Choi, D. Wang, I. T. Bae, J. Xiao, Z. Nie, W. Wang, V. V. Viswanathan, J. L. Yun, J. G. Zhang, G. L. Graff, Z. Yang and J. Liu, *Nano Lett.*, 2010, **10**, 2799.
69 J. Lloris, C. Pérez Vicente and J. L. Tirado, *Electrochem. Solid-State Lett.*, 2002, **5**, A234.
70 A. Sobkowiak, M. R. Roberts, R. Younesi, T. Ericsson, L. Häggström, C. W. Tai, A. M. Andersson, K. Edström, T. Gustafsson and F. Björefors, *Chem. Mater.*, 2013, **25**, 3020.
71 J. Barker, R. K. B. Gover, P. Burns, A. Bryan, M. Y. Saidi and J. L. Swoyer, *J. Power Sources*, 2005, **146**, 516.
72 W.-G. Ryu, H. S. Shin, M. S. Park, H. Kim, K. N. Jung and J. W. Lee, *Ceram. Int.*, 2019, **45**, 13942.
73 W. Hua, B. Schwarz, M. Knapp, A. Senyshyn, A. Missiul, X. Mu, S. Wang, C. Kübel, J. R. Binder and S. Indris, *J. Electrochem. Soc.*, 2019, **166**, A5025.
74 M. Stein IV, C. F. Chen, M. Mullings, D. Jaime, A. Zaleski, P. P. Mukherjee and C. P. Rhodes, *J. Electrochem. Energy Convers. Storage*, 2016, **13**, 031001.
75 A. Chakraborty, S. Kunnikuruvan, M. Dixit and D. T. Major, *Isr. J. Chem.*, 2020, **60**, 850.
76 L. Zhu, C. Bao, L. Xie, X. Yang and X. Cao, *J. Alloys Compd.*, 2020, **831**, 154864.
77 Q. Wang, B. Mao, S. I. Stoliarov and J. Sun, *Prog. Energy Combust. Sci.*, 2019, **73**, 95.
78 A. Manthiram, B. Song and W. Li, *Energy Storage Mater.*, 2017, **6**, 125.
79 X. Cheng, J. Zheng, J. Lu, Y. Li, P. Yan and Y. Zhang, *Nano Energy*, 2019, **62**, 30.
80 H. Sun and K. Zhao, *J. Phys. Chem. C*, 2017, **121**, 6002.
81 Q. Tao, L. Wang, C. Shi, J. Li, G. Chen, Z. Xue, J. Wang, S. Wang and H. Jin, *Mater. Chem. Front.*, 2021, **5**, 2607.
82 L. Mu, Z. Yang, L. Tao, C. K. Waters, Z. Xu, L. Li, S. Sainio, Y. Du, H. L. Xin, D. Nordlund and F. Jin, *J. Mater. Chem. A*, 2020, **8**, 17487.
83 Y. Lu, Y. Zhang, Q. Zhang, F. Cheng and J. Chen, *Particuology*, 2020, **53**, 1.
84 Y. Ruana, X. Song, Ya. Fu, C. Song and V. Battaglia, *J. Power Sources*, 2018, **400**, 539.
85 L. Wu, K.-W. Nam, X. Wang, Y. Zhou, J.-C. Zheng, X.-Q. Yang and Y. Zhu, *Chem. Mater.*, 2011, **23**, 3953.
86 B. Liu, Y. Jia, C. Yuan, L. Wang, X. Gao, S. Yin and J. Xu, *Energy Storage Mater.*, 2020, **24**, 85.
87 V. G. Bagrova, *J. Synchrotron Radiat.*, 2018, **25**, 1619.
88 D. Rouan, Synchrotron Radiation, in *Encyclopedia of Astrobiology*, ed. M. Gargaud, *et al.*, Springer, Berlin, Heidelberg, 2015.
89 P. F. Tavares, S. C. Leemann, M. Sjöström and Å. Andersson, *J. Synchrotron Radiat.*, 2014, **21**, 862.
90 S. Moniri and P. Taherparvar, *J. Instrum.*, 2019, **14**, T02001.
91 L. Filler, *Design of three bending magnets for use with beam from target to eight-inch pipe*, United States, 1968, DOI: **10.2172/1157343**.
92 G. Geloni, V. Kocharyan and E. Saldin, *J. Synchrotron Radiat.*, 2015, **22**, 288.
93 K. J. Kim, *AIP Conf. Proc.*, 1989, **184**, 565.
94 J. L. Laclare, *Nucl. Instrum. Methods Phys. Res., Sect. A*, 2001, **467–468**, 1.
95 C. A. Smith, G. L. Card, A. E. Cohen, T. I. Doukov, T. Eriksson, A. M. Gonzalez, S. E. McPhillips, P. W. Dunten, I. I. Mathews, J. Song and S. M. Soltis, *J. Appl. Crystallogr.*, 2010, **43**, 1261.
96 Y. Hirose, *R&D Rev. Toyota CRDL*, 2003, **38**, 1.
97 E. Mitchell, P. Kuhn and E. Garman, *Structure*, 1999, **7**, R111.
98 Y. U. Sohn, J.-Y. Choi, S. N. Kim, K. R. Kim, J. S. Bak and Y. M. Koo, *Nucl. Instrum. Methods Phys. Res., Sect. A*, 2001, **467–468**, 707.

99 H. Winick and G. P. Williams, *Synchrotron Radiat. News*, 1991, **4**, 23.
100 H. H. Lee, M. Kumar and H.-J. Shin, *Phys. Adv. Technol.*, 2017, **26**, 7.
101 D. Céolin, J. M. Ablett, D. Prieur, T. Moreno, M. J.-P. Rueff, T. Marchenko, L. Journel, R. Guillemin, T. Marin and M. Simon, *J. Electron Spectrosc. Relat. Phenom.*, 2013, **190**, 188.
102 P. S. Bagus, E. Ilton and C. J. Nelin, *Catal. Lett.*, 2018, **148**, 1785.
103 Y. Yang, S. Harmer and M. Chen, *Hydrometallurgy*, 2015, **156**, 89.
104 J. Yano and V. K. Yachandra, *Photosynth. Res.*, 2009, **102**, 241.
105 W. Li, M. Li, Y. Hu, J. Lu, A. Lushington, R. Li, T. Wu, T.-K. Sham and X. Sun, *Small Methods*, 2018, **2**, 1700341.
106 M. Fehse, A. Iadecola, L. Simonelli, A. Longo and L. Stievano, *Phys. Chem. Chem. Phys.*, 2021, **23**, 23445.
107 T. Alemu and F.-M. Wang, *J. Synchrotron Radiat.*, 2018, **25**, 151.
108 Y. Takata, K. Tamasaku, T. Tokushima, D. Miwa, S. Shin, T. Ishikawa, M. Yabashi, K. Kobayashi, J. J. Kim, T. Yao, T. Yamamoto, M. Arita, H. Namatame and M. Taniguchi, *Appl. Phys. Lett.*, 2001, **84**, 4310.
109 G. der Laan and A. I. Figueroa, *Coord. Chem. Rev.*, 2014, **277–278**, 95.
110 A. Q. R. Baron, Y. Tanaka, S. Goto, K. Takeshita, T. Matsushita and T. Ishikawa, *J. Phys. Chem. Solids*, 200, **61**, 461.
111 J. McBreen, *J. Solid State Electrochem.*, 2009, **13**, 1051.
112 H. Ade, X. Zhang, S. Cameron, C. Costello, J. Kirz and S. Williams, *Science*, 1992, **258**, 972.
113 J. Hilhorst, F. Marschall, T. N. Tran Thi, A. Last and T. U. Schülli, *J. Appl. Crystallogr.*, 2014, **47**, 1882.
114 F. Meirer, Y. Liu, E. Pouyet, B. Fayard, M. Cotte, C. Sanchez, J. Andrews, A. Mehta and P. Sciau, *J. Anal. At. Spectrom.*, 2013, **28**, 1870.
115 P. Fischer, D.-H. Kim, B. L. Mesler, W. Chao and E. H. Anderson, *J. Magn. Magn. Mater.*, 2007, **310**, 2689.
116 P. Tack, J. Garrevoet, S. Bauters, B. Vekemans, B. Laforce, E. V. Ranst, D. Banerjee, A. Longo, W. Bras and L. Vincze, *Anal. Chem.*, 2014, **86**, 8791.
117 K. J. Gaffney and H. N. Chapman, *Science*, 2007, **316**, 1444.
118 J. McBreen, *J. Solid State Electrochem.*, 2009, **13**, 1051.
119 M. Giorgetti, *ISRN Mater. Sci.*, 2013, **2013**, 938625.
120 P. P. R. M. L. Harks, F. M. Mulder and P. H. L. Notten, *J. Power Sources*, 2018, **288**, 92.
121 E. Talaie, P. Bonnick, X. Sun, Q. Pang, X. Liang and L. F. Nazar, *Chem. Mater.*, 2017, **29**, 90.
122 F. Lin, Y. Liu, X. Yu, L. Cheng, A. Singer, O. G. Shpyrko, H. L. Xin, N. Tamura, C. Tian, T. C. Weng, X.-Q. Yang, Y. S. Meng, D. Nordlund, W. Yang and M. M. Doeff, *Chem. Rev.*, 2017, **117**, 13123.
123 B. Bozzini and A. Goldoni, *J. Phys. D: Appl. Phys.*, 2018, **51**, 050201.
124 T. M. M. Heenan, C. Tan, J. Hack, D. J. L. Brett and P. R. Shearing, *Mater. Today*, 2019, **31**, 69.
125 S. K. Babu, A. I. Mohamed, J. F. Whitacre and S. Litster, *J. Power Sources*, 2015, **283**, 314.
126 A. V. Llewellyn, A. Matruglio, D. J. L. Brett, R. Jervis and P. R. Shearing, *Condens. Matter*, 2020, **5**, 75.
127 S. Wang, W. Hua, S. Zhou, X. He and L. Liu, *Chem. Eng. J.*, 2020, **400**, 125998.
128 H. J. Kim, J. H. Jo, J. U. Choi, N. Voronina, D. Ahn, T.-Y. Jeon, H. Yashiro, Y. Aniskevich, G. Ragoisha, E. Streltsov and S.-T. Myung, *Energy Storage Mater.*, 2021, **40**, 197.
129 J. Kim, D. Ahn, C. Kulshreshtha, K.-S. Sohn and N. Shin, *Acta Crystallogr., Sect. C: Cryst. Struct. Commun.*, 2009, **65**, i14.
130 J. I. Sohn, H. J. Joo, K. S. Kim, H. W. Yang, A.-R. Jang, D. Ahn, H. H. Lee, S. N. Cha, D. J. Kang, J. M. Kim and M. E. Welland, *Nanotechnology*, 2012, **23**, 205707.
131 S. Senbhagaraman, T. N. Guru Row and A. M. Umarji, *J. Mater. Chem.*, 1993, **3**, 309.
132 J. P. Singh, S. O. Won, W. C. Lim, I. J. Lee and K. H. Chae, *J. Mol. Struct.*, 2016, **1108**, 444.
133 S. Weber, *J. Appl. Crystallogr.*, 1997, **30**, 565.
134 G. Rodriguez and S. Rodriguez, *J. Chem. Educ.*, 1989, **66**, 648.
135 D. L. Bish and S. A. Howard, *J. Appl. Crystallogr.*, 1988, **21**, 86.
136 W. Hua, K. Wang, M. Knapp, B. Schwarz, S. Wang, H. Liu, J. Lai, M. Müller, A. Schökel, A. Missyul, D. F. Sanchez, X. Guo, J. R. Binder, J. Xiong, S. Indris and H. Ehrenberg, *Chem. Mater.*, 2020, **32**, 4984.
137 W. Lee, S. Lee, E. Lee, M. Choi, R. Thangavel, Y. Lee and W. S. Yoon, *Energy Storage Mater.*, 2022, **44**, 441–451.
138 S. Hwang, S. M. Kim, S.-M. Bak, K. Y. Chung and W. Chang, *Chem. Mater.*, 2015, **27**, 6044.
139 Z. Feng, R. Rajagopalan, S. Zhang, D. Sun, Y. Tang, Y. Ren and H. Wang, *Adv. Sci.*, 2021, **8**, 2001809.
140 P. Wang, P. Li, T.-F. Yi, H. Yu, X. Lin, S. Qian, Y. R. Zhu, M. Shui and J. Shu, *Electrochim. Acta*, 2016, **190**, 248.
141 M. Jeong, H. Kim, W. Lee, S.-J. Ahn, E. Lee and W.-S. Yoon, *J. Power Sources*, 2020, **474**, 228592.
142 N. Li, S. Sallis, J. K. Papp, B. D. McCloskey, W. Yang and W. Tong, *Nano Energy*, 2020, **78**, 105365.
143 A. O. Kondrakov, H. Geßwein, K. Galdina, L. de Biasi, V. Meded, E. O. Filatova, G. Schumacher, W. Wenzel, P. Hartmann, T. Brezesinski and J. Janek, *J. Phys. Chem. C*, 2017, **121**, 24381.
144 W. Li, H. Y. As, Q. Xie and A. Manthiram, *J. Am. Chem. Soc.*, 2019, **141**, 5097.
145 C. H Shen, Q. Wang, F. Fu, L. Huang, Z. Lin, S.-Y. Shen, H. Su, X.-M. Zheng, B.-B. Xu, J.-T. Li and S.-G. Sun, *ACS Appl. Mater. Interfaces*, 2014, **6**, 5516.
146 Y. N. Zhou, J. L. Yue, E. Hu, H. Li, L. Gu, K. W. Nam, S. M. Bak, X. Yu, J. Liu, J. Bai, E. Dooryhee, Z.-W. Fu and X.-Q. Yang, *Adv. Energy Mater.*, 2016, **6**, 1600597.
147 J. Lai, J. Zhang, Z. Li, Y. Xiao, W. Hua, Z. Wu, Y. Chen, Y. Zhong, W. Xiang and X. Guo, *Chem. Commun.*, 2020, **56**, 4886.
148 S. Gao, Y.-T. Cheng and M. Shirpour, *ACS Appl. Mater. Interfaces*, 2019, **11**, 982.

149 J. Zheng, Y. Ye, T. Liu, Y. Xiao, C. Wang, F. Wang and F. Pan, *Acc. Chem. Res.*, 2019, **52**, 2201.
150 M. Jiang, Q. Zhang, X. Wu, Z. Chen, D. L. Danilov, R.-A. Eichel and P. H. L. Notten, *ACS Appl. Energy Mater.*, 2020, **3**, 6583.
151 T. Wang, K. Ren, W. Xiao, W. Dong, H. Qiao, A. Duan, H. Pan, Y. Yang and H. Wang, *J. Phys. Chem. C*, 2020, **124**, 5600.
152 S. Wang, W. Hua, A. Missyul, M. S. D. Darma, A. Tayal, S. Indris, H. Ehrenberg, L. Liu and M. Knapp, *Adv. Funct. Mater.*, 2021, **31**, 2009949.
153 D. Wang, C. Xin, M. Zhang, J. Bai, J. Zheng, R. Kou, J. Y. P. Ko, A. Huq, G. Zhong, C. J. Sun, Y. Yang, Z. Chen, Y. Xiao, K. Amanine, F. Pan and F. Wang, *Chem. Mater.*, 2019, **31**, 2731.
154 S. Schweidler, L. de Biasi, G. Garcia, A. Mazilkin, P. Hartmann, T. Brezesinski and J. Janek, *ACS Appl. Energy Mater.*, 2019, **2**, 7375.
155 C. Xu, K. Märker, J. Lee, A. Mahadevegowda, P. J. Reeves, S. J. Day, M. F. Groh, S. P. Emge, C. Ducati, B. L. Mehdi, C. C. Tang and C. P. Grey, *Nat. Mater.*, 2021, **20**, 84.
156 Y. Kim, H. Park, K. Shin, G. Henkelman, J. H. Warner and A. Manthiram, *Adv. Energy Mater.*, 2021, **11**, 2101112.
157 N. E. Henriksen and K. B. Møller, *J. Phys. Chem. B*, 2008, **112**, 558.
158 E. Hu, S. MinBak, S. D. Senanayake, X.-Q. Yang, K.-W. Nam, L. Zhang and M. Shao, *J. Power Sources*, 2015, **277**, 193.
159 L. Wu, K.-W. Nam, X. Wang, Y. Zhou, J.-C. Zheng, X. Q. Yang and Y. Zhu, *Chem. Mater.*, 2011, **23**, 3953.
160 S. M. Bak, E. Hu, Y. Zhou, X. Yu, S. D. Senanayake, S.-J. Cho, K. B. Kim, K. Yoon Chung, X. Q. Yang and K. W. Nam, *ACS Appl. Mater. Interfaces*, 2014, **6**, 22594.
161 X. Q. Yang, X. Sun, S. J. Lee, J. McBreen, S. Mukerjee, M. L. Daroux and X. K. Xing, *Electrochem. Solid-State Lett.*, 1999, **2**, 157.
162 D. Mohanty, J. Li, S. C. Nagpure, D. L. Wood III and C. Daniel, *MRS Energy Sustain.*, 2015, **2**, e15.
163 K. W. Nam, S. M. Bak, E. Hu, X. Yu, Y. Zhou, X. Wang, L. Wu, Y. Zhu, K. Y. Chung and X. Q. Yang, *Adv. Funct. Mater.*, 2013, **23**, 1047.
164 A. L. Lipson, J. L. Durham, M. LeResche, I. A. Baker, M. J. Murphy, T. T. Fister, L. Wang, F. Zhou, L. Liu, K. Kim and D. Johnson, *ACS Appl. Mater. Interfaces*, 2020, **12**, 18512.
165 E. Penner-Hahn, in *X-ray Absorption Spectroscopy*, eLS, 2005, DOI: **10.1038/npg.els.0002984**.
166 S. Brennan and P. L. Cowan, *Rev. Sci. Instrum.*, 1992, **63**, 850.
167 A. Sharma, J. P. Singh, S. O. Won, K. H. Chae, S. K. Sharma and S. K. Gautam, Introduction to X-ray absorption spectroscopy and its applications in material science, in *Handbook of Materials Characterization*, ed. S. Sharma, Springer, Cham 2018, pp. 497–548.
168 A. Sharma, M. Varshney, W. C. Lim, H. J. Shin, J. P. Singh, S. O. Won and K. H. Chae, *Phys. Chem. Chem. Phys.*, 2017, **19**, 6397.
169 H.-N. Hwang, H.-S. Kim, B. Kim, C. C. Hwang, S. W. Moon, S. M. Chung, C. Jeon, C.-Y. Park, K. H. Chae and W. K. Choi, *Nucl. Instrum. Methods Phys. Res., Sect. A*, 2007, **581**, 850.
170 J. P. Singh, S. H. Kim, S. O. Won, I. J. Lee and K. H. Chae, *RSC Adv.*, 2018, **8**, 31275.
171 J. P. Singh and K. H. Chae, *ACS Omega*, 2019, **4**, 7140.
172 G. Ali, J.-H. Lee, B. W. Cho, K.-W. Nam, D. Ahn, W. Chang, S. H. Oh and K. Y. Chung, *Electrochim. Acta*, 2016, **191**, 307.
173 P. Thakur, V. Bisogni, J. C. Cezar, N. B. Brookes, G. Ghiringhelli, S. Gautam, K. H. Chae, M. Subramanian, R. Jayavel and K. Asokan, *J. Appl. Phys.*, 2010, **107**, 103915.
174 N. Zhang, X. Long, Z. Wang, P. Yu, F. Han, J. Fu, G. X. Ren, Y. Wu, S. Zheng, W. Huang, C. Wang, H. Li and X. Liu, *ACS Appl. Energy Mater.*, 2018, **1**, 5968.
175 I.-J. Lee, C.-J. Yu, Y.-D. Yun, C.-S. Lee, I. D. Seo, H.-Y. Kim, W.-W. Lee and K. H. Chae, *Rev. Sci. Instrum.*, 2010, **81**, 026103.
176 S.-M. Bak, Z. Shadike, R. Lin, X. Yu and X.-Q. Yang, *NPG Asia Mater.*, 2018, **10**, 563.
177 C.-J. Chang, Y. Zhu, J. Wang, H.-C. Chen, C.-W. Tung, Y.-C. Chu and H. M. Chen, *J. Mater. Chem. A*, 2020, **8**, 19079.
178 R. Dominko, I. Arčon, A. Kodre, D. Hanžel and M. Gaberščček, *J. Power Sources*, 2009, **189**, 51.
179 G. Aquilanti, M. Giorgetti, R. Dominko, L. Stievano, I. Arcon, N. Novelo and L. Olivi, *J. Phys. D: Appl. Phys.*, 2017, **50**, 074001.
180 R. S. Liu, L. Y. Jang, J. M. Chen, Y. C. Tsai, Y. D. Hwang and R. G. Liu, *J. Solid State Chem.*, 1997, **128**, 326.
181 H. Wadati, D. G. Hawthorn, T. Z. Regier, G. Chen, T. Hitosugi, T. Mizokawa, A. Tanaka and G. A. Sawatzky, *Appl. Phys. Lett.*, 2010, **97**, 022106.
182 A. Ito, Y. Sato, T. Sanada, M. Hatano, H. Horie and Ya. Ohsawa, *J. Power Sources*, 2011, **196**, 6828.
183 A. Deb, U. Bergmann, S. P. Cramer and E. J. Cairns, *J. Appl. Phys.*, 2005, **97**, 113523.
184 K. M. Shaju, G. V. S. Rao and B. V. R. Chowdari, *Electrochim. Acta*, 2002, **48**, 145.
185 Z. Chen, J. Wang, B. Tom, L. Bai, S. Chen, Y. Zhao, T. Sum, J. Lin and Z. Shen, *Sci. Rep.*, 2016, **6**, 25771.
186 K. R. Tallman, G. P. Wheeler, C. J. Kern, E. Stavitski, X. Tong, K. J. Takeuchi, A. C. Marschilok, D. C. Bock and E. S. Takeuchi, *J. Phys. Chem. C*, 2021, **125**, 58.
187 C. Tian, Y. Xu, D. Nordlund, F. Lin, J. Liu, Z. Sun, Y. Liu and M. Doeff, *Joule*, 2018, **2**, 464.
188 Xi. Liu, D. Wang, G. Liu, V. Srinivasan, Z. Liu, Z. Hussain and W. Yang, *Nat. Commun.*, 2013, **4**, 2568.
189 Y. W. Tsai, B. J. Hwang, G. Ceder, H. S. Sheu, D. G. Liu and J. F. Lee, *Chem. Mater.*, 2005, **17**, 3191.
190 K. Kubobuchi, M. Mogi, M. Matsumoto, T. Baba, C. Yogi, C. Sato, T. Yamamoto, T. Mizoguchi and H. Imai, *J. Appl. Phys.*, 2016, **120**, 142125.
191 A. Iadecola, A. Perea, L. Aldon, Gi. Aquilanti and L. Stievano, *J. Phys. D: Appl. Phys.*, 2017, **50**, 144004.
192 Qi. Li, R. Qiao, L. A. Wray, J. Chen, Z. Zhuo, Y. Chen, S. Yan, F. Pan, Z. Hussain and W. Yang, *J. Phys. D: Appl. Phys.*, 2016, **49**, 413003.
193 T. Liu, L. Yu, J. Liu, J. Lu, X. Bi, A. Dai, M. Li, M. Li, Z. Hu, L. Ma, D. Luo, J. Zheng, T. Wu, Y. Ren, J. Wen, F. Pan and K. Amine, *Nat. Energy*, 2021, **6**, 277.

194 F. Frati, M. O. J. Y. Hunault and F. M. F. de Grooet, *Chem. Rev.*, 2020, **120**, 4056.
195 C. Liang, W. Zhang, Z. Wei, Z. Wang, Q. Wang and J. Sun, *J. Energy Chem.*, 2021, **59**, 446.
196 J. P. Singh, J. Y. Park, K. Hwa Chae, D. Ahn and S. Lee, *Nanomaterials*, 2020, **10**, 459.
197 S. Koo, J. Lee, J. Lee, S. Yoon and D. Kim, *Energy Storage Mater.*, 2021, **42**, 764.
198 J. Hong, W. E. Gent, P. Xiao, K. Lim, D.-H. Seo, J. Wu, P. M. Csernica, C. J. Takacs, D. Nordlund, C.-J. Sun, K. H. Stone, D. Passarello, W. Yang, D. Prendergast, G. Ceder, M. F. Toney and W. C. Chueh, *Nat. Mater.*, 2019, **18**, 256.
199 G. H. Lee, J. Wu, D. Kim, K. Cho, M. Cho, W. Yang and Y.-M. Kang, *Angew. Chem.*, 2020, **132**, 8759.
200 A. D. Dwivedi, N. D. Sanadiya, J. P. Singh, S. M. Husnain, K. H. Chae, D. S. Hwang and Y. S. Chang, *ACS Sustainable Chem. Eng.*, 2017, **5**, 518.
201 V. Singh, A. K. Paidi, C.-H. Shim, S. H. Kim, S. O. Won, J. P. Singh, S. Lee and K. H. Chae, *Crystals*, 2021, **11**, 490.
202 J. P. Singh, W. C. Lim, S. O. Won, J. Song and K. H. Chae, *J. Korean Phys. Soc.*, 2018, **72**, 890.
203 K. V. Klementiev, VIPER, freeware, *J. Phys. D: Appl. Phys.*, 2001, **34**, 209.
204 M. Newville, *J. Phys.: Conf. Ser.*, 2013, **430**, 012007.
205 J. Timoshenko, A. Kuzmin and J. Purans, *Comput. Phys. Commun.*, 2012, **183**, 1237.
206 B. Ravel and M. Newville, *J. Synchrotron Radiat.*, 2005, **12**, 537.
207 M. Newville, *Rev. Mineral. Geochem.*, 2014, **78**, 33.
208 Z. Sun, W. Yan, T. Yao, Q. Liu, Y. Xie and S. We, *Dalton Trans.*, 2013, **42**, 13779.
209 S. D. Kelly, D. Hesterberg and B. Ravel, *Methods of soil analysis part 5 mineralogical methods*, Soil Science Society of America, Madison, 2008, ch. 14.
210 D. C. Koningsberger, B. L. Mojet, G. E. Van Dorssen and D. E. Ramaker, *Top. Catal.*, 2000, **10**, 143.
211 E. Curis, J. Osan, G. Falkenberg, S. Benazeth and S. Torok, *Spectrochim. Acta*, 2015, **60**, 841.
212 E. Curis and S. Bénazeth, *J. Synchrotron Radiat.*, 2015, **12**, 361.
213 C. Yin, Z. Wei, M. Zhang, B. Qiu, Y. Zhou, Y. Xiao, D. Zhou, L. Yun, C. Li, Q. Gu, W. Wen, X. Li, X. Wen, Z. Shi, L. He, Y. S. Meng and Z. Liu, *Mater. Today*, 2021, **51**, 15–26.
214 S. Kaewmala, W. Limphirat, V. Yordsri, H. Kim, S. Muhammad, W.-S. Yoon, S. Srilomsak, P. Limthongkul and N. Meethong, *Sci. Rep.*, 2019, **9**, 427.
215 A. Ito, Y. Sato, T. Sanada, T. Ohwaki, M. Hatano, H. Horie and Y. Ohawa, *Electrochemistry*, 2010, **78**, 380.
216 S. Tao, W. Huang, S. Chu, B. Qian, L. Liu and W. Xu, *Mater. Today Phys.*, 2021, **18**, 100403.
217 P. Yan, J. Zheng, Z.-K. Tang, A. Devaraj, G. Chen, K. Amine, J.-G. Zhang, L.-M. Liu and C. Wang, *Nat. Nanotechnol.*, 2019, **14**, 602.
218 S.-K. Jung, H. Gwon, J. Hong, K.-Y. Park, D.-H. Seo, H. Kim, J. Hyun, W. Yang and K. Kang, *Adv. Energy Mater.*, 2014, **4**, 1300787.
219 Y. Su, Q. Zhang, L. Chen, L. Bao, Y. Lu, Q. Shi, J. Wang, S. Chen and F. Wu, *ACS Appl. Mater. Interfaces*, 2020, **12**, 37208.
220 L. Li, J. Chen, H. Huang, L. Tan, L. Song, H.-H. Wu, C. Wang, Z. Zhao, H. Yi, J. Duan, T. Dong, E. Lee, S. Muhammad, T. Kim, H. Kim, W. Lee and W.-S. Yoon, *Adv. Sci.*, 2020, **7**, 1902413.
221 J. Lim, S. Y. Park, J. Y. Huang, S. M. Han and H. T. Kim, *Rev. Sci. Instrum.*, 2013, **84**, 013707.
222 J. Lim, H. Kim and S. Y. Park, *J. Synchrotron Radiat.*, 2014, **21**, 827.
223 B. E. Etschmann, E. Donner, J. Brugger, D. L. Howard, M. D. de Jonge, D. Paterson, R. Naidu, K. G. Scheckel, C. G. Ryan and E. Lombi, *Environ. Chem.*, 2014, **11**, 341.
224 M. Katayama, K. Sumiwaka, K. Hayashi, K. Ozutsumi, T. Ohta and Y. Inada, *J. Synchrotron Radiat.*, 2012, **19**, 717.
225 J. Y. Park, J. P. Singh, J. Lim and S. Lee, *J. Synchrotron Radiat.*, 2020, **27**, 545.
226 J. Wang, Y. C. Karen Chen-Wiegert and J. Wang, *Nat. Commun.*, 2014, **5**, 4570.
227 F. Wang, S. Lou, S. Li, Z. Yu, Q. Liu, A. Dai, C. Cao, M. F. Toney, M. Ge, X. Xiao, W. K. Lee, Y. Yao, J. Deng, T. Liu, Y. Tang, G. Yin, J. Lu, D. Su and J. Wang, *Nat. Commun.*, 2020, **11**, 3050.
228 Z. Xu, Z. Jiang, C. Kai, R. Xu, C. Qin, Y. Zhang, M. M. Rehman, C. Wei, D. Nordlund, C. J. Sun, X. Xiao, X. W. Du, K. Zhao, P. Yan, Y. Liu and F. Lin, *Nat. Commun.*, 2020, **11**, 83.
229 J. Y. Park, J. P. Singh, J. Lim, K. H. Chae and S. Lee, *Mater. Lett.*, 2020, **261**, 126983.
230 J. Le Houx and D. Kramer, *Energy Reports*, 2021, **7**, 9.
231 J. Y. Park, Y. Kim, S. Lee and J. Lim, *J. Synchrotron Radiat.*, 2020, **27**, 1696.
232 L. R. Brandt, J.-J. Marie, T. Moxham, D. P. Förstermann, E. Salvati, C. Besnard, C. Papadaki, Z. Wang, P. G. Bruce and A. M. Korsunsky, *Energy Environ. Sci.*, 2020, **13**, 3556.
233 M. Jiang, D. L. Danilov, R.-A. Eichel and P. H. L. Notten, *Adv. Energy Mater.*, 2021, **11**, 2103005.
234 J. Chen, W. Deng, X. Gao, S. Yin, L. Yang, H. Liu, G. Zou, H. Hou and X. Ji, *ACS Nano*, 2021, **15**, 6061.
235 W. Hua, B. Schwarz, R. Azmi, M. Müller, M. S. D. Darma, M. Knapp, A. Senyshyn, M. Heere, A. Missyul, L. Simonelli, J. R. Binder, S. Indris and H. Ehrenberg, *Nano Energy*, 2020, **78**, 105231.
236 J. P. Singh, J. Y. Park, A. K. Paidi, Y. Lee, J. Lim, K. H. Chae, D. Ahn and S. Lee, Probing Origin of First Cycle Irreversibility in the Ni-Rich Layered Oxide Cathode Materials: Role of Porosity and Chemical State Heterogeneity, communication.
237 D. Sung, D. Nam, M.-j. Kim, S. Kim, K. S. Kim, S.-Y. Park, S. M. Hwang, C. Jung, H. Lee, D. H. Cho, M. Kim, I. Eom, S. Yong Lee, C. Song and S. Kim, *Appl. Sci.*, 2021, **11**, 5082.
238 J.-W. Lee, M. Kim, G. Kang, S. M. Vinko, L. Bae, M. S. Cho, H.-K. Chung, M. Kim, S. Kwon, G. Lee, C. H. Nam, S. H. Park, J. H. Sohn, S. H. Yang, U. Zastrau and B. I. Cho, *Phys. Rev. Lett.*, 2021, **127**, 175003.

239 I. Eom, S. H. Chun, J. H. Lee, D. Nam, R. Ma, J. Park, S. Park, S. H. Park, H. Yang, I. Nam, M. H. Cho, C. H. Shim, G. Kim, C.-K. Min, H. Heo, H.-S. Kang and C. Kim, *Appl. Sci.*, 2022, **12**, 1010.

240 I. Nam, C.-K. Min, B. Oh, G. Kim, D. Na, Y. J. Suh, H. Yang, M. H. Cho, C. Kim, M.-J. Kim, C. H. Shim, J. H. Ko, H. Heo, J. Park, J. Kim, S. Park, G. Park, S. Kim, S. H. Chun, H. J. Hyun, J. H. Lee, K. S. Kim, I. Eom, S. Rah, D. Shu, K.-J. Kim, S. Terentyev, V. Blank, Y. Shvyd'ko, S. J. Lee and H.-S. Kang, *Nat. Photonics*, 2021, **15**, 435.